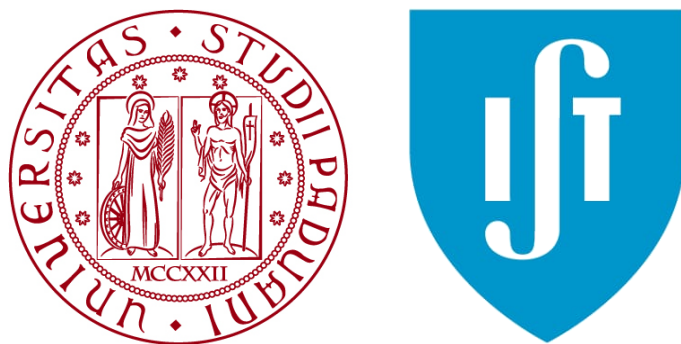


UNIVERSITÀ DEGLI STUDI DI PADOVA
DIPARTIMENTO DI INGEGNERIA INDUSTRIALE DII
Department Of Industrial Engineering

INSTITUTO SUPERIOR TÉCNICO
DEPARTAMENTO DE ENGENHARIA ELETROTÉCNICA E DE COMPUTADORES DEEC
Department of Electrical and Computer Engineering

Corso di Laurea Magistrale in Ingegneria dell'Energia Elettrica



TESI DI LAUREA

Evaluation of wireless charging systems from the point of view of energy transfer in electric mobility

Relatori:

Dott.ssa Patrícia Baptista
(Instituto Superior Técnico – Lisbona)

Dott. Gonçalo Duarte
(Instituto superior de engenharia de Lisboa – Lisbona)

Prof. Roberto Turri

Laureando:
Mattia Minelli

2027132

Abstract

The ongoing electrification of the mobility sector has pushed the companies to look for new solutions to improve the EV experience of the clients. The electric technology is not yet mature enough to guarantee a comfortable use because of the limited range and the long charging times. A possible solution to these problems could be represented by the Dynamic Wireless Charging Systems (DWCS).

After a brief overview of the technology and of the related state of the art in the first two chapters, the work focus on its two targets:

- Modeling a DWCS via MATLAB/Simulink
- Analysing the influence of the main parameters

Chapter 3 explains the assumption made to assemble the model, from the grid to the DD coils and then to the battery of the vehicle. The SAE Standard J2954 is the reference.

In the following chapter different trip-scenarios are simulated by varying the average speed, the available power, the distance between the transmitting coils and the misalignment of the vehicle and comparing the results.

Chapter 5 shows the conclusions and the possible future improvements.

Table of Contents

1.	Introduction	12
1.1	EV market	12
1.2	Types of Electric Vehicles	13
1.3	Battery Technology in EVs	14
1.4	Battery Management System	15
1.5	Charging Modes in EVs	16
1.6	Benefits of WPT	19
1.7	Objectives	20
2.	Wireless Power Transfer	22
1.8	Introduction	22
1.9	Inductive WPT	24
1.10	Magnetic Resonance WPT	26
1.11	Capacitive WPT	27
1.12	Compensation topologies	28
1.13	WPT Operation Modes	30
1.14	Static vs. dynamic WCS	31
1.15	Standards for EV Wireless Chargers: SAE J2954	32
1.16	Coils geometry and materials	33
1.17	Wireless Power Transfer Market perspectives	37
3.	Methodology	40
1.18	Tools of the study	40
1.19	Structure of the model	40
1.20	Wireless charging system	43
1.1.1	Off-board – Ground assembly (GA)	44
1.1.2	Mutual coupling (M)	48

1.1.3	On-board - Vehicle assembly (VA)	54
1.21	Power, energy, overall efficiency	56
1.22	Scenarios	58
4.	Results	62
1.23	Validation of the model	62
1.24	Influence of average speed (U_{avg})	66
1.25	Influence of available power (P_g)	69
1.26	Influence of track coverage ratio (ϵ)	70
1.27	Influence of Horizontal misalignment (K_y)	71
5.	Conclusions and future work	75
1.28	Conclusions and limitations of the model	75
6.	References	79

Table of Figures

Figure 1.1 - Different characteristics for EVs (source [3])	15
Figure 1.2 - Diagram of a BMS (source [3])	16
Figure 1.3 - Battery charging process in the CC-CV mode (Source: [3])	18
Figure 2.1 – Main features of WPT systems (Source [3])	24
Figure 2.2 – generic diagram of a wpt system (source [3])	24
Figure 2.3 – Equivalent circuit of WPT systems (Source [3])	25
Figure 2.4 - Generic diagram for magnetic resonance wireless chargers with compensation networks (Source [3])	27
Figure 2.5 - Generic diagram for capacitive wireless chargers with compensation networks (Source [3])	28
Figure 2.6 - Equivalent circuit of Series compensation. (a) Series–Series. (b) Series–Parallel topology (Source [21])	29
Figure 2.7 - Equivalent circuit of Parallel compensation. (a) Parallel–Parallel topology (b) Parallel–Series topology (Source [21])	29
Figure 2.8 - Equivalent circuits of hybrid compensation topologies. (a) LCC-LCC, (b) CCL-LC, (c) LCLLCCL and (d) LC-LC (Source [21])	30
Figure 2.9 - WPT operation modes (Source [3])	30
Figure 2.10 – example of circular and rectangular coils (source: [3])	34
Figure 2.11 - DD, DDQ and bipolar coils (Source [3])	34
Figure 2.12 - Lumped coil (on top) vs. Stretched coil (Source [3])	36
Figure 2.13 - Section of a Litz wire	37
Figure 3.1 - Scheme of the model	41
Figure 3.2 -- Example of drive cycle	42
Figure 3.3 - Typical functional elements of a wireless charging system (Source [28])	43
Figure 3.4 - Wireless charging system parts	43
Figure 3.5 - Off-board section of WCS	44
Figure 3.6 - Concentrated WPT system configuration (Source: [27])	45
Figure 3.7 - Three-phase thyristor rectifier (Source: [43])	46
Figure 3.8 - Full bridge single-phase inverter (Source: [43])	47
Figure 3.9 - Configuration of the coils	50
Figure 3.10 - Typical shape of M with longitudinal misalignment	50
Figure 3.11 - ε vs. D	52

Figure 3.12 - M/M ₀ vs. y-offset for DD coils	53
Figure 3.13 - K _y vs. y-offset	53
Figure 3.14 - On-board section of WCS	54
Figure 3.15 - Single-phase diode rectifier (Source: [46])	55
Figure 3.16 - KIA EV6 Air (Source: [49])	57
Figure 3.17 - Rua Carlos da Maia-Avenida de Madrid (Source: [50])	58
Figure 3.18 - Speed profile of the first journey and WCS activation	58
Figure 3.19 - Saldanha (Lisbon) – Loures (Source: [50])	59
Figure 3.20 - Speed profile of the second journey and WCS activation	59
Figure 3.21 - Lumiar - Campo de Ourique (Source: [50])	60
Figure 3.22 - Speed profile of the third journey and WCS activation	60
Figure 4.1 - Total consumed energy (black), Energy from charger (blue) and Net consumed energy (orange) in the first journey	66
Figure 4.2 - Total consumed energy (black), Energy from charger (blue) and Net consumed energy (orange) in the second journey	67
Figure 4.3 - Total consumed energy (black), Energy from charger (blue) and Net consumed energy (orange) in the third journey	68
Figure 4.4 - χ vs. D	71
Figure 4.5 - Energy from charger vs. y-offset	72
Figure 4.6 - χ vs. y-offset	72
Figure 4.7 - y-offset vs. speed	73

Table of Tables

Table 1.1: - EV characteristics (source [3])	13
Table 1.2 - Charging mode approaches (source: [10])	19
Table 2.1 - Properties of WPT technologies (Source [3])	28
Table 2.2 - Comparison of Static and dynamic WCS (Source [27])	32
Table 2.3 - SAE J2954 WPT power classifications (*still under study) (Source: [28])	33
Table 2.4 - – Specification of the SAE J2954 VA Z-classes (Source [28])	33
Table 2.5 - - Positioning tolerance requirements for Test Stand VAs and Product VAs (Source: [3])	33
Table 2.6 - Comparison between the different geometries (Source [3])	35
Table 3.1 - SAE J2954 WPT power classifications (*still under study) (Source: [28])	45
Table 3.2 - Off board values of the model	48
Table 3.3 - Specification of the SAE J2954 VA Z-classes (Source: [28])	48
Table 3.4 - Mechanical dimensions of the Product VA WPT3/Z2 (Source: [28])	49
Table 3.5 - – Mechanical dimensions of the Product GA WPT3 (Source: [28])	49
Table 3.6 - VA coil inductance (Source: [28])	49
Table 3.7 - GA coil inductance (Source: [28])	49
Table 3.8 - Coupling k between GA and VA coil for Z2 class (Source: [28])	49
Table 3.9 - Assumptions for the model (Source: [28])	49
Table 3.10 - ϵ vs. D	51
Table 3.11 - Mutual coupling values of the model	54
Table 3.12 - VA/on-board values of the model	55
Table 3.13 - Minimum system efficiency requirements (Source: [28])	57
Table 3.14 - KIA EV6 Air characteristics (Source: [49])	57
Table 3.15 - Information about the journey Rua Carlos da Maia-Avenida de Madrid in Lisbon (Source: [50])	58
Table 3.16 – Information about the journey Saldanha (Lisbon) – Loures (Source: [50])	59
Table 3.17 - Information about the journey Lumiar – Campo de Ourique (Source: [50])	60
Table 4.1 - Inputs and outputs of example [3]	62
Table 4.2 - Inputs and outputs of the model	63
Table 4.3 - Deviations from example [3]	63
Table 4.4 - Inputs and outputs of example [48]	64
Table 4.5 - Inputs and outputs of the model	65

Table 4.6 - Input and output values of the model (SAE J2954 parameters)	66
Table 4.7 - Resuming table of the energies in the first simulation	67
Table 4.8 - Resuming table of the energies in the second simulation	67
Table 4.9 - Resuming table of the energies in the second simulation	68
Table 4.10 - Comparison between the simulations	68
Table 4.11 - Upscaled charging systems parameters, energies and χ	70
Table 4.12 - Different values of χ for different available grid powers (Pg)	70
Table 4.13 - – Different ϵ for different D	70
Table 4.14 - Ky effect on energy transfer	72
Table 4.15 - χ value with y-offset based on speed (Avg = average)	73
Table 5.1 - Resume table of the different parameters (\uparrow = “if...increases”, \downarrow = “if...decreases”)	76

Acronyms

- AC:** Alternate current
D: Distance between tracking coils
DD: Double D (coils)
DC: Direct current
DWCS: Dynamic wireless charging system
 ϵ : Track coverage ratio
E: Energy
EV: Electric vehicle
f: Frequency
GA: Ground assembly
HF: High frequency
HV: High voltage
I: Current
 I_p : Pick-up current
 I_t : Tracker current
k: Coupling coefficient
 K_y : Horizontal alignment coefficient
L: Self-inductance
LL: Line to line
LN: Line to neutral
LV: Low voltage
M: Mutual inductance
MV: Medium voltage
 η : efficiency
p: Pick-up
 P_g : Available grid power
 P_c : Charging power
PF: Power factor
pk: Peak
 P_t : Tracker input power
 R_L : Load resistance

RMS: Root mean square

SWCS: Static wireless charging system

t: Tracker

T: Time

U: Speed

U_{avg} : Average speed

V: Voltage

V_p : Pick-up voltage

V_t : Tracker voltage

VA: Vehicle assembly

WCS: Wireless charging system

WPT: Wireless power transfer

x: Collected energy ratio

X_t : Length of the coil

ω : Pulsation

1. Introduction

Due to the ongoing environmental crisis the governments of the majority of the countries are relying on a renewable revolution and on the electrification of the transportation system which nowadays is responsible for a big share of carbon dioxide emissions worldwide.

The transition to a fully electrified mobility is accelerating now, putting the focus on new storage and charging solutions. Here is an overview of batteries and EVs.

1.1 EV market

As explained in [1] the electric car market is one of the most rapidly developing sectors in clean energy, with electric vehicle (EV) sales reaching an all-time high of 6.6 million in 2021 - double the number sold in the previous year. This is a significant increase from the mere 120,000 electric cars sold worldwide in 2012. In addition, electric cars accounted for almost 10% of global car sales in 2021 - four times the market share in 2019 - resulting in a total of approximately 16.5 million electric cars on the world's roads, which is triple the number in 2018.

The remarkable success of electric vehicles (EVs) can be attributed to several factors. The primary factor is the continuous support from policies, which is the main driving force. In 2021, public expenditure on subsidies and incentives for EVs doubled, reaching almost USD 30 billion. A growing number of countries have made commitments to phase out internal combustion engines or have set ambitious targets for vehicle electrification in the coming decades. Moreover, many car manufacturers have plans to electrify their fleets that go beyond policy targets. Finally, the number of new EV models available in the market has increased by five times in 2021 compared to 2015, which has enhanced their appeal to consumers. As of now, around 450 models of EVs are available in the market.

In 2021, the surge in EV sales was mainly driven by China, which accounted for half of the growth. In fact, more electric vehicles were sold in China in 2021 (3.3 million) than in the entire world in 2020. Sales in Europe also exhibited strong growth, with a 65% increase to 2.3 million, following the 2020 boom. Meanwhile, in the United States, EV sales increased to 630,000 after two years of decline. The first quarter of 2022 showed similar trends, with China contributing to most of the global growth by more than doubling its sales compared to the first quarter of 2021, while the United States saw a 60% increase, and Europe recorded a 25% increase in sales. [1]

1.2 Types of Electric Vehicles

As a result of the current climatic crisis, governments and private organizations are investing in the development of EV technologies to reduce emissions and promote sustainable transportation. One of the key challenges in the development of EVs is the limited range and long charging time.

As explained in [2], vehicles can be classified as:

- BEV (Battery Electric Vehicle) - These vehicles run exclusively on electricity stored in batteries, with no internal combustion engine (ICE) or fuel cell on board.
- HEV (Hybrid Electric Vehicle) - These vehicles have both an electric propulsion system and an ICE. The electric propulsion system operates together with the ICE, increasing its efficiency.
- PHEV (Plug-in Hybrid Electric Vehicle) - These vehicles also have both an electric propulsion system and an ICE, but the electric storage system can be charged externally by plugging it into an electrical outlet.

It is important to note that the classification of EVs is constantly evolving as new technologies are developed and adopted. The classification above is based on the IEC standard but other classifications exist in some countries or by some organizations. Table 1.1 shows the characteristics of some EV models.

Model	Vehicle type	Battery size (kWh)	Energy available (kWh)	Range (km)	Energy consumption (kWh/km)
Nissan Leaf	EV	39.5	37	240	0.165
Toyota RAV4	EV	41.8	32.18	160	0.20
Volkswagen Golf-e	EV	35.8	32	190	0.168
BMW i3	EV	33	27.2	200	0.13
Tesla Model 3 standard range	EV	55	46	310	0.148
Tesla Model S performance	EV	100	95	510	0.186
Audi e-tron	EV	95	83.6	360	0.232
Chevrolet Volt	PHEV	17.1	13.7	64	0.21
Toyota Prius	PHEV	8.8	7	40	0.175
Mitsubishi Outlander	PHEV	13.8	11	37	0.29
BMW 530e	PHEV	9.2	8	34	0.237

TABLE 1.1: - EV CHARACTERISTICS (SOURCE [3])

1.3 Battery Technology in EVs

The main energy source for electric vehicles (EVs) is batteries, but some types of EVs also use other energy components. EVs can rely solely on electric propulsion or also include an internal combustion engine. [2] has classified electric vehicles based on their battery usage. Battery Electric Vehicles (BEVs) rely entirely on batteries, while Hybrid Electric Vehicles (HEVs) and Plug-in Hybrid Electric Vehicles (PHEVs) also use a combination of batteries and other energy sources. BEVs generally have a higher battery capacity than PHEVs and PHEVs have a higher battery capacity than HEVs. Batteries are used as the main storage element in EVs, storing energy in chemical form and converting it to electrical energy when needed. The performance of the batteries, such as energy density and power, is determined by the technology used. While many technologies meet the criteria for EVs, power may be a limiting factor for certain tasks such as acceleration and regenerative braking. This limitation can be overcome by incorporating other technologies such as supercapacitors.

The battery technology used in electric vehicles has evolved over time, especially in recent years with the increasing number of vehicle manufacturers in this market. The main technologies can be classified as follows:

- Lead-acid battery, the initial battery utilized to initiate the internal combustion engines in automobiles was the. While some companies like Toyota and General Motors have tried this technology in Battery Electric Vehicles (BEVs), the lead-acid battery's inadequate energy density makes it unsuitable for all-electric vehicles.
- ZEBRA batteries, also known as molten salt batteries, have been used in some vehicle concepts and urban bus models [4], but they require high operating temperatures (between 270 and 350°C).
- NiMH technology is widely used in the market for HEVs and PHEVs due to its good energy and power density, simplicity, low cost, and useful lifetime despite its lower efficiency and slightly higher weight compared to other technologies. [5]
- Lithium-ion batteries are currently the leading technology, due to their high energy and power density, and their ability to be used in a wide range of automotive applications. There are several different types of Li-ion batteries, each with their own specific chemical combination at the anode and cathode. Some of the most common types used in electric vehicles include lithium-nickel-manganese-cobalt (NMC),

lithium-nickel-cobalt-aluminium (NCA), and lithium-iron phosphate (LFP), compared in [6] (Figure 1.1). These batteries have various advantages such as longer lifespan, high specific energy, good power density, safe performance and less degradation over time. However, it is important to note that Li-ion batteries will experience some capacity loss over time with each charging and discharging cycle.

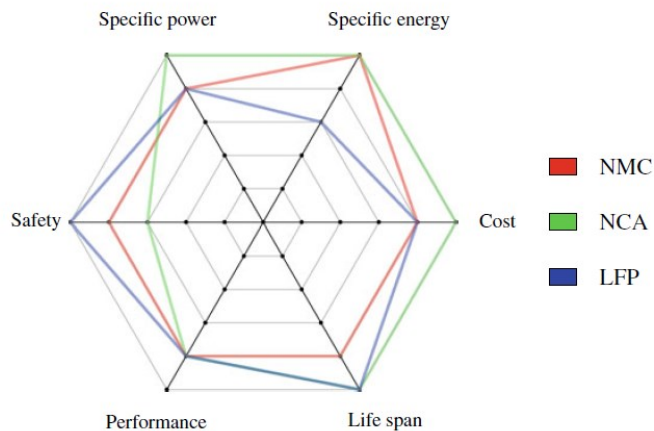


FIGURE 1.1 - DIFFERENT CHARACTERISTICS FOR EVs (SOURCE [3])

When designing a charging system for electric vehicles, it is important to consider the type of battery being used. Different types of batteries, such as Lithium-ion, NMC, NCA, and LFP, offer varying levels of energy density, efficiency, safety, lifespan, and cost [7].

While NMC batteries are commonly used in EV applications due to their high energy density and reasonable performance, NCA batteries have become more cost-effective thanks to reduced cobalt usage. On the other hand, LFP batteries are suitable for heavy vehicles due to their long lifespan and safe operation, even though they have a lower energy density. It is also important to note that batteries can be modelled as an equivalent resistance during charging, with the resistance value depending on the battery's power and voltage/current specifications.

1.4 Battery Management System

In order to ensure the safe operation of an EV battery, a Battery Management System (BMS) is implemented. The BMS monitors and controls various parameters such as voltage, temperature, State of Charge (SoC), State of Health (SoH), input current and output current to ensure that the charge and discharge process of the Lithium-ion battery is done in compliance with safety requirements. [7] If there are dangerous conditions that could potentially damage the battery, the BMS activates protection circuits, such as Cut-off Field

Effect Transistors (FETs), to disconnect the battery from other electrical circuits and protect it from over-current, over-voltage, overheating, or abrupt discharge which can greatly reduce the battery's lifespan.

The BMS plays an important role in managing the charge and discharge of the battery in an EV. It controls the current and voltage in each of the battery's cells, which store energy in an electrochemical format that can be easily converted to electrical energy. The BMS also monitors and balances the cell voltages to prolong the battery's lifetime. The BMS can also disconnect the battery from other electrical circuits as a safety measure. Some BMS systems use a separate controller for charging and discharging, while others use a single controller for both processes.

Figure 1.2 shows a diagram of a typical BMS in which the same controller is responsible for the charge and discharge of this storage element.

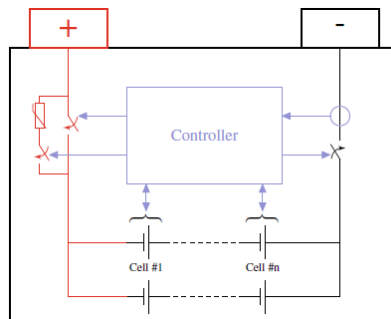


FIGURE 1.2 - DIAGRAM OF A BMS (SOURCE [3])

1.5 Charging Modes in EVs

The batteries can be charged in different ways, defined by SAE (Society of Automotive Engineers) Standard J1772 [8]:

- Level 1. It provides charging through an AC plug at 240V, which corresponds to a standard household plug. Thus, it does not require prior installation of any specific electrical equipment to charge the vehicle.
- Level 2. Charging is achieved through an AC plug at 240 V and 40 A.
- Level 3. In contrast to previous levels, here the charging process is performed using DC current instead of AC current. The output voltage is 480 V.

An alternative classification of the methods to charge an EV battery is provided by the IEC 61851 standard [9]. Specifically, four modes are defined:

- Mode 1 involves charging with a maximum voltage of 250 V and a maximum current of 16 A, providing a maximum power of 3.7 kW. It uses a conventional household plug but is not recommended for prolonged use due to the risk of overheating.
- Mode 2 also uses a conventional plug but includes a protection system to monitor the power of the charge/discharge and to incorporate a communication scheme. The maximum current allowed in this mode is 32 A. The connection of the plug to the grid is Schuko whereas in the vehicle it is typically Mennekes.
- Mode 3 requires a specific installation, known as a wallbox, which is connected to the grid and implements control and protection functionalities. It also incorporates an active communication channel between the charging point and the car, making it the most appropriate equipment to install for smart grids.
- Mode 4 involves charging in DC power transfer. A wallbox connected to the grid transforms the AC power to DC. It also includes protection and control mechanisms, and is intended for fast charging, with a maximum current of 400 A and a maximum power of 240 kW. The main drawback is that it is an expensive equipment.

The transfer of power from the grid to the vehicle is defined by previously discussed levels and modes. Additionally, the vehicle's battery may have specific requirements for voltage and/or current during charging. As a result, the charging process of the battery can be completed using one of the following four configurations:

- Constant-Current (CC) charging: In this method, a constant current is applied to the battery throughout the charging process. This current rate is typically low to extend the battery's lifespan. However, this approach results in a longer charging time. The charge is completed when the charging time reaches a predefined duration, based on the current and battery capacity. Both NiMH and Li-ion batteries can be charged using this method.
- Constant-Voltage (CV) charging: In this method, a predefined constant voltage is applied to the battery during charging. The advantage of this approach is that overvoltages and associated damages are avoided, which can help to extend the battery's

lifespan. The current is gradually decreased until it reaches a predefined value, at which point the charging is considered complete.

- Constant-Current–Constant-Voltage (CC–CV) charging: This charging method consists of two phases. In the first phase, a constant current is applied, set according to the manufacturer's recommendations and the maximum current the battery can tolerate without damage. The voltage increases during this phase. When the voltage reaches its maximum, the charging mode switches to a constant voltage mode. The current is gradually decreased in this second phase. The charging is considered complete when the current drops to a predefined value. This charging mode, which is the most widely used for EV batteries, is illustrated in Figure 1.3.

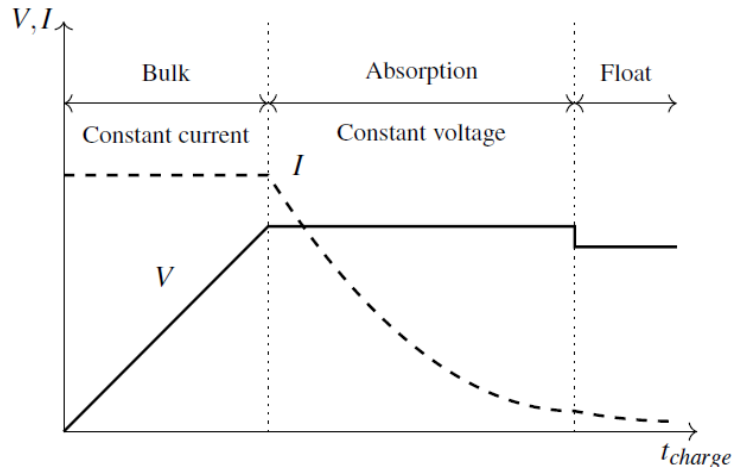


FIGURE 1.3 - BATTERY CHARGING PROCESS IN THE CC-CV MODE (SOURCE: [3])

- Multi-stage constant current (MCC) charging: this approach involves charging the battery in multiple phases or stages. In each phase, a constant current is applied, with the value depending on the phase. The phase changes to a different current when the voltage reaches a threshold, also specific to the phase. The main advantage of this mode is that it can offer a shorter charging time, making it ideal for fast chargers. However, it can be challenging to optimize the parameters for each phase, such as the current and threshold voltage.

A comparison of the charging approaches is presented in [10], as shown in Table 1.2.

Mode	Advantages	Disadvantages	Key elements
CC	Easy to implement	Capacity utilization is low	• Charging constant current rate; • Terminal condition
CV	• Easy to implement; • Stable terminal voltage	Easy to cause the lattice collapse of battery	• Charging constant voltage; • Terminal condition
CC–CV	• Capacity utilization is high; • Stable terminal voltage	Difficult to balance objectives such as charging speed, energy loss, temperature variation	• Constant current rate in CC phase; • Constant voltage in CV phase; • Terminal condition
MCC	• Easy to implement; • Easy to achieve fast charging	Difficult to balance objectives such as charging speed, capacity utilization and battery lifetime	• The number of CC stages; • Constant current rates for each stage

TABLE 1.2 - CHARGING MODE APPROACHES (SOURCE: [10])

1.6 Benefits of WPT

Even though EVs have benefits for the environment and energy consumption, some drivers are hesitant to use them due to concerns about reduced autonomy. To encourage more widespread adoption of EVs, new methods that are convenient and user-friendly are necessary. In this context, Wireless Power Transfer (WPT) technology is a promising solution for EV charging. The main benefits of WPT for EVs include [11]:

- Autonomous operation. The charging and discharging process can be completed without the driver involvement. This feature is particularly useful for Vehicle-to-Grid (V2G) applications, where the driver can participate in the electrical market without any need of manual configuration.
- Safe charging. The driver is not required to handle an electrical conductor, eliminating the risk of high current contact. Additionally, the energy transfer is secure in challenging weather conditions like snow or rain.
- Flexible charging. WPT expands the charging options for EVs, allowing them to charge while in motion or parked for a short period. If this type of charging becomes common, it could mean that EV batteries can be smaller, and the vehicle can use less expensive electrical equipment. These benefits are relevant for all types of EVs including cars, bicycles, buses, trains, boats, and drones. The most advanced implementation of wireless chargers for EVs uses magnetic resonance technology,

including commercial devices for static charging and prototypes for stationary and dynamic charging.

As explained previously, magnetic resonance WPT is the predominant technology in EV wireless chargers. The main challenge to address is obtaining an acceptable power transfer efficiency with a relevant gap and even when misalignment occurs. This must be done in compliance with safety considerations.

1.7 Objectives

The objectives of the work are essentially two:

- **Modeling a dynamic wireless charging system via MATLAB/Simulink**, in which the challenge is keeping it as closer as possible to a real system.
- **Analysing the influence of the main parameters**, to figure out if systems like these can be feasible.

2. Wireless Power Transfer

The chance of removing the conductor would largely simplify the charging process, thereby opening to a world of new possibilities for EVs.

Explaining the state of the art, the potential and the possible implementations of this kind of technology is the goal of the following chapter.

1.8 Introduction

Wireless Power Transfer (WPT) is a technology that enables the transfer of power without the use of physical conductors. It uses electromagnetic waves, generated by one or multiple transmitters, which are then received by one or several receivers to store to feed a device or simply to store the energy in a battery. The concept was first explored by Nikola Tesla in the late 19th century [12], but it wasn't until the 21st century that the technology saw renewed interest due to big improvements in power converters. WPT technology can now be found in a variety of commercial products, such as electric toothbrushes, power mats for mobile phones, and electric vehicle chargers. The market for WPT is expected to continue growing, with predictions of over 2.2 billion units sold by 2023 [13] and revenues of nearly 17.9 billion dollars by 2024. [14]

WPT applications can be classified based on various criteria, such as the type of electromagnetic wave used, the distance between the transmitter and receiver, and the type of receiver [3]. Figure 2.1 shows an example of how WPT systems can be classified according to these criteria.

- Transferred power: which can be low power (up to 1 kW), medium power (1-100 kW) or high power (more than 100 kW). The power requirement of the application greatly affects the system design. For low-power applications, the primary aim is to transfer the maximum power possible, whereas for higher-power applications, efficiency becomes more crucial.
- Power direction: uni-directional systems are those where the power transfer is always provided by a fixed element with a source connected. In these systems, the power flows in one direction only. On the other hand, bi-directional systems allow

for the load (such as a battery or capacitor) to occasionally provide energy back to the source. These systems allow power to flow in both directions.

- Gap: distance between the energy transmitter and the receiver. Some WPT systems require a direct contact between the transmitter and receiver, such as power mats. However, in other applications, the transmitter and receiver can be separated by several centimeters or meters. This distance between transmitter and receiver is known as "gap."
- Intermediate objects: ability to operate with intermediate objects in the gap between the transmitter and receiver. Some technologies are not able to operate with intermediate objects due to the wavelength, others may suffer a significant degradation when these objects are present, and others may not be affected.
- Number of transmitters: a basic WPT system consists of one power transmitter and one power receiver. However, multiple transmitters can be deployed in a region to transfer power to a load. In this case, more than one transmitter can be activated simultaneously, considering their power availability and the efficiency of the power transfer. For mobile loads, the role of power transfer can be executed by different transmitters in different time intervals.
- Number of receivers: typically, a WPT system consists of one power transmitter and one power receiver. However, some configurations support multiple loads, allowing multiple receivers to benefit from the power generated by one transmitter.
- Mobility of the receiver: in some applications, the receiver may be placed in a random position before the charging process begins, such as in dynamic EV wireless charging. These systems are designed to handle mobility of the receiver and are called as Mobile receiver WPT systems. On the other hand, in some applications the receiver is fixed in a specific position and the systems are called Stationary receiver WPT systems.
- Medium: most current WPT products operate with an air gap between the transmitter and receiver, but the technology can also be applied in other mediums such as water [15], ground [16], or biological tissue [17]. The medium can have a

significant impact on the efficiency, as it can affect the power transmission losses. For example, studies have shown that the efficiency of an underwater WPT system is up to 5% lower than an air-gap system [15].



FIGURE 2.1 – MAIN FEATURES OF WPT SYSTEMS (SOURCE [3])

1.9 Inductive WPT

In all the experiments and developments in wireless power transfer, the technology relies on an electromagnetic wave that travels from the power emitter to the power receiver to transfer power.

Figure 2.2 illustrates a generic diagram of a WPT system, which consists of the power source, a transmitter and a receiver separated by a distance d (known as the gap) and the load. The electromagnetic waves used in WPT systems are characterized by their wavelength λ or their frequency f .

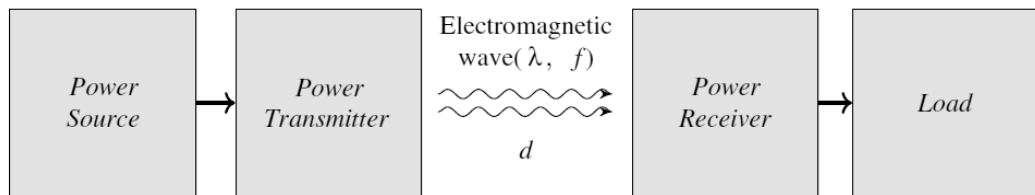


FIGURE 2.2 – GENERIC DIAGRAM OF A WPT SYSTEM (SOURCE [3])

As stated in [3] inductive WPT utilizes the magnetic field of the electromagnetic wave. It is based on the interaction of the magnetic and electrical behaviour described by Ampère's Law and Faraday's Law. According to Ampère's Law, a current-carrying wire generates a magnetic

field around it. The intensity and orientation of the magnetic field depend on the topology of the wire. The equation for Ampère's Law states that:

$$I [A] = \oint H dl \quad (2.1)$$

where H is the magnetic field intensity of the magnetic field generated by the current I and dl is the differential element of length along the path on which the current travels. This means that the frequency at which the intensity of the magnetic field varies is equal to the frequency of the current in the wire.

Faraday's Law states that when a time-varying current passes through a coil, a time-varying magnetic field is generated around it. If this time-varying magnetic field passes through another coil, a voltage (e_{ind}) is induced across its terminals. This phenomenon is described by Faraday's Law as follows:

$$e_{ind}[V] = -\frac{d\varphi}{dt} \quad (2.2)$$

Where φ is the flux of the magnetic field passing through the area limited by the coil. The combination of these two phenomena forms the basis of inductive and other magnetic-based WPT technologies. Inductive WPT technology uses a pair of coils known as the primary and secondary coils, as illustrated in Figure 2.3. The primary coil must have a time varying current generated by a generator.

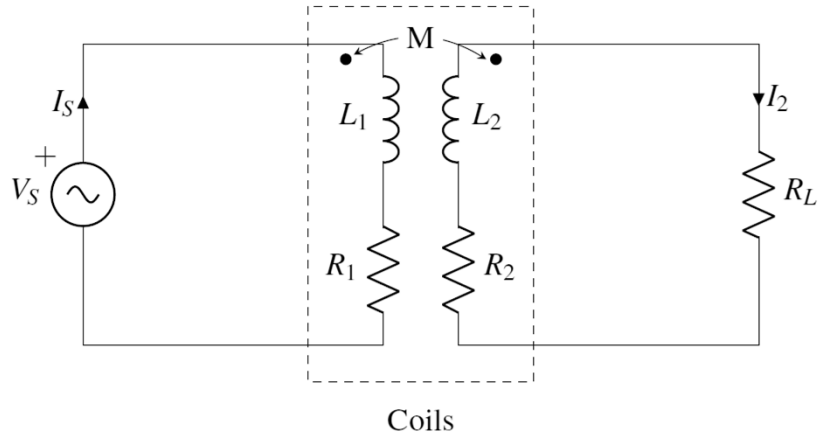


FIGURE 2.3 – EQUIVALENT CIRCUIT OF WPT SYSTEMS (SOURCE [3])

The magnetic field generated by the primary coil must pass through the area of the secondary coil to which the load (R_L) is connected. There are usually intermediate electronic components between the generator and the primary coil, and other electric systems between the secondary coil and the load. These additional elements are included to improve the efficiency of the wireless power transfer. The best approach is to produce an induced

voltage that is as high as possible. According to Faraday's Law, the induced voltage is proportional to the rate of change of the flux traversing the secondary coil. This means that a coil traversed by two magnetic fields with the same magnitude but different frequencies at two distinct moments will experience two different induced voltages. When the magnetic field passing through the coil has the highest frequency, it results in a higher induced voltage. Therefore, for inductive-based WPT, it is important to hold two conditions:

- Most of the magnetic field generated by the primary coil traverses the secondary coil (High coupling).
- The frequency of the magnetic field involved in the WPT is as high as possible (High frequency).

The first condition implies that larger coils are preferable on the secondary side, but practical limitations such as size, weight, and cost can be an issue in certain applications, particularly in biomedical and EV applications. Increasing the size of the coils can be problematic for biomedical applications due to size and weight constraints, and for EV applications, the size of the coils is limited by the structures in which the WPT components must be inserted and the cost of the materials. It is worth noticing that inductive WPT is not currently supported for EV applications, but advanced technologies based on this kind of magnetic WPT.

To enhance WPT in inductive systems, the main strategy is to increase the frequency of the electrical current in the primary coil, which leads to an increase in the frequency of the magnetic field and the rate of flux change. Power converters are used in magnetic-based WPT systems to increase the operational frequency.

1.10 Magnetic Resonance WPT

As stated in [3] magnetic resonance or resonant WPT is an improvement over inductive WPT, in which the electrical system is designed to work under resonant conditions. To meet this requirement, the pair of coils is connected to structures composed of reactive elements such as capacitors or additional coils, known as compensation networks. Figure 2.4 shows the generic diagram of a resonant WPT system.

Wireless charging in EVs is based on this technology.

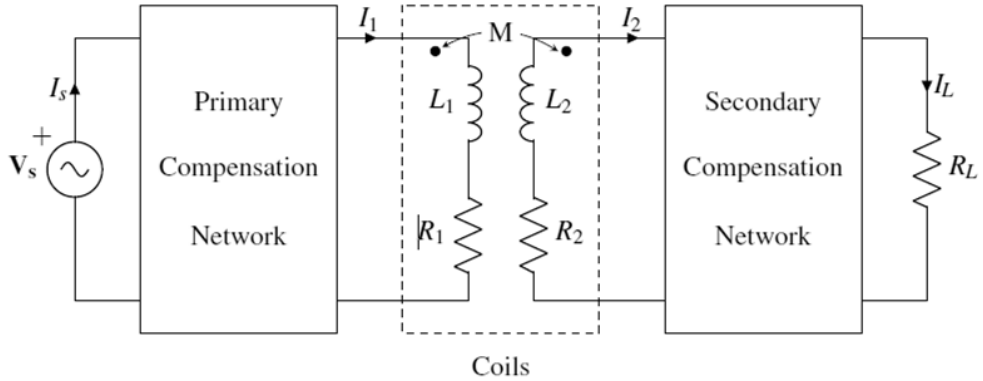


FIGURE 2.4 - GENERIC DIAGRAM FOR MAGNETIC RESONANCE WIRELESS CHARGERS WITH COMPENSATION NETWORKS (SOURCE [3])

1.11 Capacitive WPT

Capacitive WPT, in contrast to the previous WPT techniques, is achieved by means of the electrical field. To work with a capacitive WPT, two metallic plates are inserted in the power emitter and the receiver. In each part, one plate is connected to each end of the conductors connecting the power source or the load, as shown in Figure 2.5. The plates in each end of the emitter are parallel with the corresponding plates in the receiver. When the two pairs of plates are close enough, they act as two capacitors and, consequently, the electrical circuit is closed. The capacitors are identified as the forward and the return capacitors. Under these circumstances, capacitive coupling takes place. Thus, an electric field is generated between the plates and, as a result, an electrical current is induced in the power receiver. Similarly, to the magnetic-based WPT, the current induced in the power receiver is proportional to the rate of change of the electric field flux between the two pairs of plates. To increase this rate, the operational frequency is elevated from the power provided by the grid. Power converters are utilized for this purpose.

Differently from the previous technologies, Capacitive WPT has the big advantage of being able to transfer power even with intermediate objects [18]. The presence of these objects does not impact on the objects and on the integrity of the objects too.

Another advantage lies in the fact that the electric field is restricted to the region between the two plates, so that there is no dispersion.

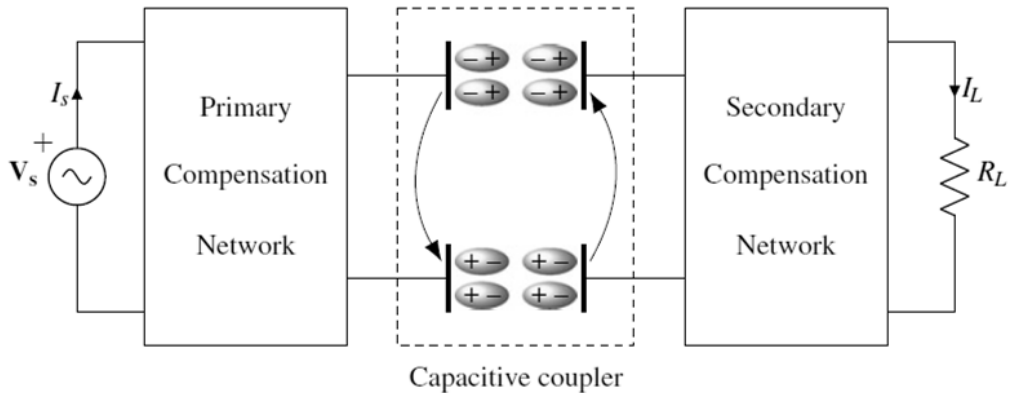


FIGURE 2.5 - GENERIC DIAGRAM FOR CAPACITIVE WIRELESS CHARGERS WITH COMPENSATION NETWORKS (SOURCE [3])

Table 2.1 compares the different kind of aforementioned technologies [3].

WPT technologies		Key advantages	Potential disadvantages
Near field	Capacitive	<ul style="list-style-type: none"> Medium power transfer up to several kilowatts Transfer even with metal objects between the transmitter and the receiver It relies on metal plates to transfer power, which are cheap components Suitable for small size applications with a reduced gap (up to 10 cm) Electric field restricted to the area between the plates: no need for controlling EMI 	<ul style="list-style-type: none"> Efficiency at the range of 70–80% The amount of power transfer is highly dependent of the gap Reduced gap (up to 10 cm)
	Inductive	<ul style="list-style-type: none"> Simple implementation for low power applications Galvanic isolation provided Simple control 	<ul style="list-style-type: none"> Limited efficiency at the range of 20% Short transmission gap (up to several cms) Need for controlling the electromagnetic emissions Highly dependent on the presence of obstacles (especially the metallic ones) in the area between the transmitter and receiver and its surroundings
	Resonant	<ul style="list-style-type: none"> High power transfer up to several kilowatts Mature technology with commercial applications already Power transfer is enabled even with some variations on the receiver's position (although the efficiency decreases) Galvanic isolation provided 	<ul style="list-style-type: none"> Expensive components for high power applications Highly dependent on the presence of obstacles (especially the metallic ones) in the area between the transmitter and receiver and its surroundings Need for controlling the electromagnetic emissions

TABLE 2.1 - PROPERTIES OF WPT TECHNOLOGIES (SOURCE [3])

1.12 Compensation topologies

Unlike pure inductive chargers, magnetic resonance technology utilizes reactive structures within the primary and secondary coils to enable the system to function under resonant conditions [3]. Due to the dimensions of the coils, the parasitic capacitance is not sufficient to ensure the resonance in the operational frequency range. Consequently, additional reactive structures, known as the compensation networks, are incorporated into the system.

The reactive components of the compensation network can be arranged with different topologies leading to other benefits in some specific configurations. As shown in [19], the most significant functionalities are:

- Reduced need for control system. Some compensation topologies make the system work as a CC or CV output. Thereby high changes in the load, for example during the charging process, do not affect the system which is more tolerant. As a result, the control part of the charging system can be simplified.
- Reduced losses. The biggest effect of the compensation networks is to resonate with the coils reducing so the reactive power supplied. When used in wireless chargers for electric vehicles, these networks are engineered to enhance both the efficiency and the power transfer capacity [20].

The simplest topologies for compensation networks opt for just one capacitor connected in series (Figure 2.6) or parallel (Figure 2.7) and that resonates with the inductance of the corresponding coil at only one frequency (mono-resonant).

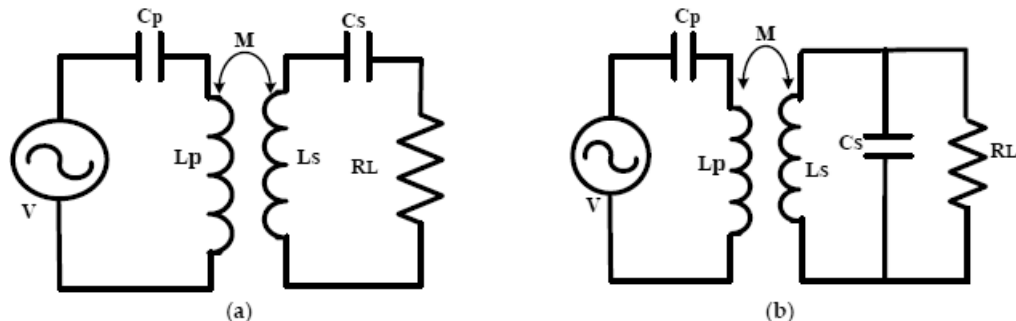


FIGURE 2.6 - EQUIVALENT CIRCUIT OF SERIES COMPENSATION. (A) SERIES-SERIES. (B) SERIES-PARALLEL TOPOLOGY (SOURCE [21])

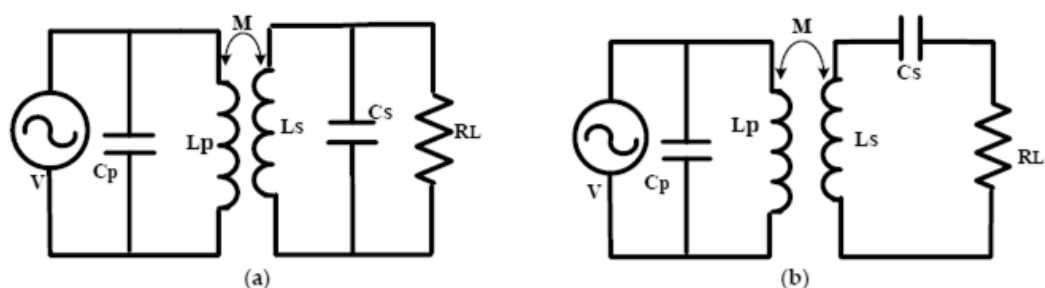


FIGURE 2.7 - EQUIVALENT CIRCUIT OF PARALLEL COMPENSATION. (A) PARALLEL-PARALLEL TOPOLOGY (B) PARALLEL-SERIES TOPOLOGY (SOURCE [21])

The alternative is represented by more complex structures with more reactive elements that can resonate at different frequencies (multi-resonant). Some examples are shown in Figure 2.8.

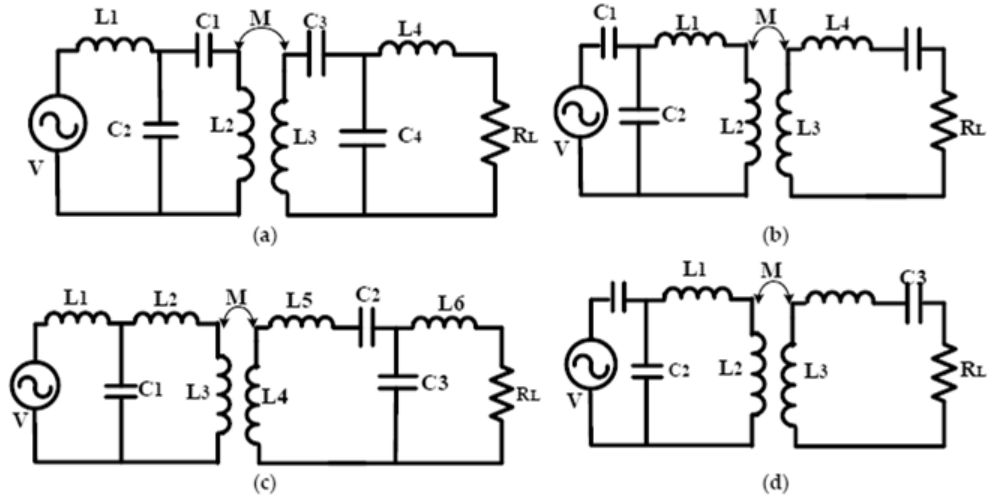


FIGURE 2.8 - EQUIVALENT CIRCUITS OF HYBRID COMPENSATION TOPOLOGIES. (A) LCC-LCC, (B) CCL-LC, (C) LCLLCCL AND (D) LC-LC
(SOURCE [21])

1.13 WPT Operation Modes

Wireless chargers increase the charging options for EVs, allowing them to charge not only when parked, but also when temporarily stopped or even moving. This can lead to reduced costs and weight for the battery as the capacity can be decreased. There are three main operation modes for wireless charging: static, stationary, and dynamic. These modes are illustrated in Figure 2.9.

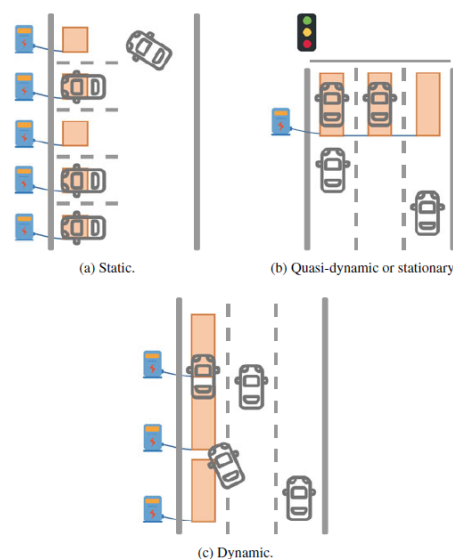


FIGURE 2.9 - WPT OPERATION MODES (SOURCE [3])

Static WPT takes place when the charge is done in a fixed location and the vehicle is expected to be turned off during the charging process. This is the case with home chargers or those found in parking lots. These chargers can include advanced features such as a control function that guides the vehicle on where to park to avoid coil misalignment. Bombardier has developed a magnetic-resonance charger for buses in Berlin that provides 200 kW in a static operation mode [22].

Another type of WPT charge is the quasi-dynamic or stationary charge. This type of charge takes place when the vehicle is stationary, but the engine is still running, and it only lasts for a short period of time which is not enough to reach a full charge. This type of charge is useful for public transport vehicles to receive energy when they stop at bus or tram stops or taxi stands. An example of this type of charge is the route-63 bus trial in Mannheim, Germany in 2013 [23]. The bus was able to charge its battery while picking up passengers without interrupting its service to recharge. The bus lane was modified to allow for this operation. Similarly, private vehicles could also be recharged during stops caused by traffic lights or regular traffic patterns.

A significant operation mode in WPT for EVs is the dynamic mode, which refers to charging that occurs while the vehicle is moving, as it travels on a paved road. Specifically, certain sections of certain lanes would be equipped with electronics to enable WPT for private use or public transport vehicles such as buses or trams. This type of charging promotes the Roadway Powered Electric Vehicle (RPEV) [24]. Dynamic charging has already been tested in some cities in South Korea, through the OLEV project, and in Spain through the Victoria project. In Turin, Italy, Conductix-Wampfler has implemented a prototype to charge a bus when stopping and at the end of the bus route using magnetic resonance technology [25].

1.14 Static vs. dynamic WCS

In [26] there is a comparison between static and dynamic wireless charging modes. Since the range of an electric vehicle is significantly limited by the battery capacity and charging speed, most of the current EVs are therefore not suitable for long distance travel. Studying their charging technology is fundamental in order to find the best solution and be able to properly reconfigure the current road infrastructure to support more electric vehicles.

Category	Fast Station	Dynamic
Waiting time	Long (>20 mins)	Zero
Battery size	Large	Small
Vehicle cost	High	Low
Infrastructure cost	High	High

TABLE 2.2 - COMPARISON OF STATIC AND DYNAMIC WCS (SOURCE [27])

The advantages of dynamic over static charging technology are cited in [26] (Table 2.2):

- Increased range: as vehicles are continuously charged while driving, range anxiety is theoretically eliminated, which cannot be achieved by any other existing technology and infrastructure.
- Improved transport lightness and safety: as vehicles can be recharged more frequently (“snack” charging), the size and weight of the on-board battery pack is significantly reduced. In addition, electric vehicles are continuously connected to the network and better share traffic information.
- Reduced demand from the power grid: the dynamic charging system is built along the roadway and the load is distributed more evenly compared to a fast-charging station.

1.15 Standards for EV Wireless Chargers: SAE J2954

Manufacturers of EV wireless chargers must ensure that their products are interoperable and comply with international standards to ensure safe and efficient charging at any charging site. Two main organizations, SAE in the US and the IEC in Europe, are currently working on developing specifications for EV wireless chargers. SAE published the third version of SAE J2954 in 2020 [28] and IEC established standards through the IEC 61980 [29].

The Society of Automotive Engineers (SAE) is an international organization based in the United States that focuses on developing international standards, particularly in the transportation industry. Through the SAE J2954 Recommended Practice specification, the organization aims to ensure interoperability among unidirectional EV wireless chargers in stationary applications. The specification defines classes of EV wireless chargers and sets requirements for minimum efficiency. It also includes descriptions of testing systems that are based on magnetic-resonance WPT for this type of charger.

In 2016, SAE published the first version of the document titled "Wireless Power Transfer for Light-Duty Plug-In/Electric Vehicles and Alignment Methodology" and an updated version was released in 2020. The document outlines four types of chargers and provides a summary of their features, as presented in Table 2.3.

	WPT1	WPT2	WPT3	WPT4*	WPT5*
Range of Input Volt-Amps [kVA]	0 to 3.7	0 to 7.7	0 to 11.1	0 to 22	0 to 60

TABLE 2.3 - SAE J2954 WPT POWER CLASSIFICATIONS (*STILL UNDER STUDY) (SOURCE: [28])

In Table 2.4, the distance between the two coils is referred to as the Vehicle Assembly (VA) coil-ground clearance. The document defines three types of operation, known as Z-classes, for this parameter. In the Z1-class, the gap ranges from 100 to 150 mm, in the Z2-class it can vary from 140 to 210 mm, and in the Z3-class the distance is between 170-250 mm.

Z-class	VA Coil Ground Clearance Range [mm]
Z1	100 to 150
Z2	140 to 210
Z3	170 to 250

TABLE 2.4 -- SPECIFICATION OF THE SAE J2954 VA Z-CLASSES (SOURCE [28])

Other operational parameters are defined, such as the frequency that can range between 81.38 kHz and 90 kHz and the ability to work in misalignment conditions as shown in Table 2.5.

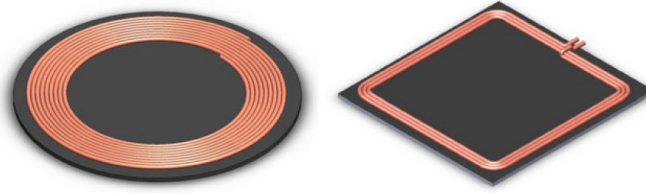
OFFSET DIRECTION	Value [mm]
ΔX	± 75
ΔY	± 100
ΔZ	Specified by manufacturer

TABLE 2.5 -- POSITIONING TOLERANCE REQUIREMENTS FOR TEST STAND VAs AND PRODUCT VAs (SOURCE: [3])

1.16 Coils geometry and materials

While a few suggestions have been put forward regarding 3D coil designs [30], the majority of designs utilized in EV WPT planar coils. Typically, this is the norm for the pick-up coil, as explained in the following subsection. However, for high-power applications where a

ferromagnetic material surrounds the track coil, the transmitter coil may become bulky. Initially, basic coil structures were used to support the first EV wireless chargers. Specifically, circular and rectangular coils were the most commonly utilized options (Figure 2.10).



(a) Circular coil.

(b) Rectangular coil.

FIGURE 2.10 – EXAMPLE OF CIRCULAR AND RECTANGULAR COILS (SOURCE: [3])

The coil design has a significant influence on system efficiency. Coils with high quality factors can improve system efficiency by up to 20% [31]. Coil geometry is another factor to consider. When coupled coils experience lateral misalignment, it causes fluctuations in their mutual inductance. Research conducted in [32], [33], reveals that the mutual inductance of rectangular coils is lower than that of circular coils. Nonetheless, rectangular coils demonstrate better resistance to coil misalignment than circular ones.

Despite their simplicity, circular and rectangular coils continue to be utilized today. However, other more intricate geometries have been proposed to reduce sensitivity to coil misalignment. These include the DD, the DDQ, and the bipolar coils, all of which are illustrated in Figure 2.11.

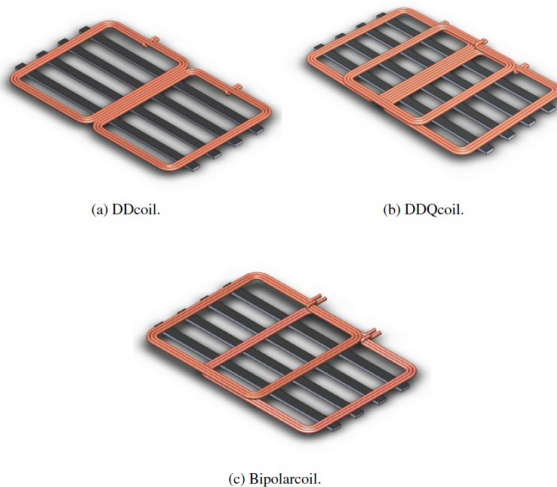


FIGURE 2.11 - DD, DDQ AND BIPOLAR COILS (SOURCE [3])

The Double-D (DD) coils consist of two identical D-shaped (rectangular) sub-coils connected in parallel with a shared side, as outlined in [34]. The winding direction of each coil is opposite to one another so that the current flows clockwise in one sub-coil and counterclockwise in the other. From a magnetic perspective, they are considered to be in series, but they have a parallel electrical connection. Since the two sub-coils are in contact, the magnetic fields produced by one coil affect the other, resulting in mutual coupling between the two sub-coils.

The DDQ or DD quadrature employs two separate windings: the first one follows the DD pattern, while the second coil, called the quadrature or Q coil, overlaps half of the area of each D component. These coils are typically supported by a ferrite and metallic structure underneath, ensuring that the DD and Q coils are not coupled. The self-inductance of the D-coil and the quadrature coil may differ, and the design process can be performed independently. This topology provides excellent flexibility to handle misalignments and interoperability, but it complicates the power electronics and its control as there are two subsystems to manage. [35]

Coils structure	Misalignment tolerant	Coefficient of coupling	EMF exposure	Effect of shielding on coefficient of coupling	Magnetic flux
Circular pad	Poor	Low	High	Low	Single sided
DD coil	Poor	High	Low	High	Double sided
DDQ coil	High	High	Low	High	Double sided
Bipolar pad	Medium	High	Low	High	Double sided

TABLE 2.6 - COMPARISON BETWEEN THE DIFFERENT GEOMETRIES (SOURCE [3])

The structure of a bipolar coil is also based on D-shaped coils that are equivalent to those used in DD coils. However, unlike DD coils, one of the coils in a bipolar coil overlaps only half of the area of the other D-shaped coil. This can be viewed as a middle ground between DD and DDQ coils, as it can capture more magnetic flux than DD coils but less than DDQ coils. Furthermore, because of its simpler geometry, the cost and loss associated with copper are lower than those for DDQ coils [36].

A comparison between the different geometries is shown in Table 2.6.

Dynamic wireless charging applications can use two different geometries for the primary coil, also known as the track coil, as illustrated in Figure 2.12. The first approach involves a track coil with dimensions similar to that of the pickup coil installed in electric vehicles (EVs). Multiple track coils are placed along a lane to ensure a sustained charging process over a

reasonable distance. In contrast, the stretch coils have a longitudinal dimension that is much larger than the size of the pickup coils.

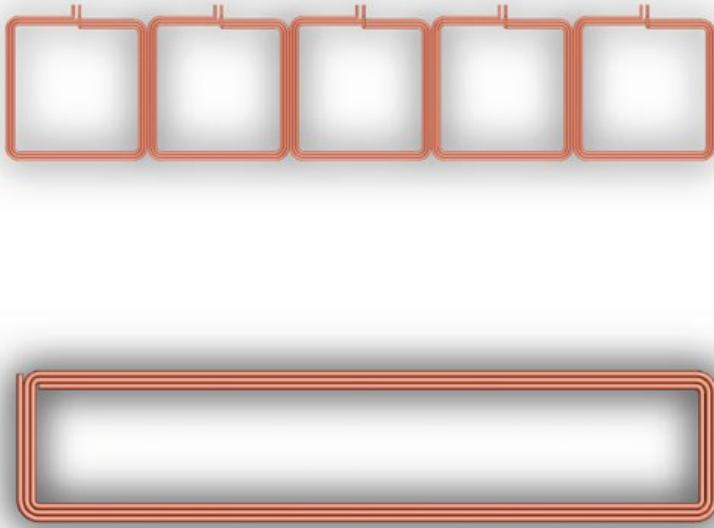


FIGURE 2.12 - LUMPED COIL (ON TOP) VS. STRETCHED COIL (SOURCE [3])

The main advantage of the lumped system is that it is possible to activate single coils when the pick-up coil is approaching (instead of all the track) reducing the wasted electromagnetic fields and increasing so the efficiency. On the other hand, this configuration is more expensive.

To improve the overall efficiency of the wireless charger, it is advisable to use a wire material with low resistance for the coils. This is because reduced losses in the inductors can minimize power dissipation increasing the overall efficiency of the wireless charger [11].

The equivalent resistance of a wire is dependent on both its length and operational frequency. Therefore, two terms are defined to describe the losses: DC and AC winding loss. The DC losses are primarily due to the resistivity of the conductor, whereas the AC losses are caused by the eddy current effects. The eddy current effects combine two phenomena: the skin and the proximity effects [37].

Skin effect describes the tendency of AC current flowing through a conductor to be concentrated near the surface of the conductor. As the frequency increases, the current becomes more concentrated in the "skin" of the conductor, causing a reduction in the effective cross-section of the cable. On the other hand, proximity effect is caused by parallel conductors carrying current. The current flowing in one conductor generates a magnetic field, which then alters the current concentration in the parallel conductors. Specifically, the

current tends to concentrate in the areas furthest away from the conductor generating the initial magnetic field.

AC winding losses result in a non-uniform current density, which reduces the effective area through which the current flows. This non-uniformity is non-linearly dependent on the frequency. To minimize AC winding losses, Litz wire is used in EV wireless chargers. Litz wire consists of multiple insulated parallel strands, with the DC resistance of each strand being equivalent. These insulated strands are twisted to form a bundle, and then multiple bundles are twisted together to create a bundle of bundles. Figure 2.13 illustrates a section of a Litz wire.



FIGURE 2.13 - SECTION OF A LITZ WIRE

The purpose of using Litz wire is to achieve a uniform current density. In order to achieve this, the diameter of the strands should be varied to obtain a uniform current density at the switching frequency and its harmonics. The diameter of the bundle should also be adjusted to achieve uniformity at the fundamental frequency. If these two parameters are set correctly, the effective area of a Litz wire is much higher than that of a solid-round wire, making the skin effect negligible. This is explained in [38].

1.17 Wireless Power Transfer Market perspectives

The market for wireless EV charging in transportation is expected to grow positively due to factors like consumer preference for convenience, need for charging infrastructure and the reliability and efficiency of the technology.

Currently, North America is the leading market for wireless transfer applications, but the Asia Pacific region is projected to become the dominant market for wireless EV charging systems by 2025. The European Union is also expected to see significant growth in demand for these

systems from 2020 to 2024. The market is seeing a surge in the availability of wireless EV chargers from a variety of sources, including start-ups, established technology providers, and car manufacturers. Among the different types of wireless EV charging, dynamic charging is expected to see the fastest growth in the period from 2020 to 2025 [39], [40].

Wireless EV technology providers are forming partnerships with EV manufacturers to establish business models, prove commercial reliability, and explore potential market opportunities. The level of technology maturity varies among providers, with some companies at the prototype testing and development stage, while others have already deployed their solutions.

- In 2007 WiTricity was born as a start-up at MIT. It develops wireless power solutions using magnetic resonance technology. WiTricity is one of the leading technology providers in the wireless application market. It works with EV car manufacturers and suppliers to deploy EV wireless charging. Following its recent acquisition of the Qualcomm Halo IP portfolio, WiTricity reinforced its role as a reference provider of wireless charging technology to car manufacturers. WiTricity's 3.6–11 kW EV charging products show an overall system efficiency of 90–93% [3]. WiTricity works actively with global standardisation agencies such as SAE International and IEC/ISO. The WiTricity EV wireless products offer several charging rates varying from 3.6 to 11 kW to meet different EV battery needs and with a single system design; this means that WiTricity products can charge vehicles from low to high ground clearance cars. WiTricity is a member of the AirFuel Alliance. This consortium is formed by industry leaders focused on fostering the transition to wireless power technology. This association is working on wireless charging standards including magnetic resonance to improve user experience. Its goal is to establish a holistic environment for developing inter-operability and open standards that help accelerate innovation and drive the marketplace forward.
- In 2011, Qualcomm purchased the "Halo" technology from the University of Auckland, which now serves as the foundation for its dynamic electric vehicle charging test track. Utilizing magnetic resonance, Qualcomm's Halo technology links power from the electric infrastructure to the EV pad integrated into the vehicle charging system. Additionally, the Qualcomm Halo system is equipped with Vehicle-to-Grid technology, allowing it to transfer energy from the electric vehicle battery to the electricity grid. The technology delivers a power rate of 3.3 to 20 kW with an

overall efficiency of more than 90%, employing a patented innovative technology that ensures highly efficient power transfer, even when the charging pads are not perfectly aligned. In February 2019, WiTricity acquired Qualcomm Inc.'s Halo wireless charging business, which included more than 1,500 patents and applications related to wireless charging. WiTricity intends to integrate Qualcomm Halo into its own wireless charging operations. [3]

- Evatran's Plugless Level 2 EV Charging System is a wireless electric vehicle charging system that has been successfully operating in the market [3]. In 2011, Evatran initiated field trials for Plugless, with installations in various locations across the United States, including pilots at Google, SAP, and Hertz. Since its first production system was shipped in early 2014, Plugless units have provided over 1 million charge hours without any issues. The United States Department of Energy and the Swedish Energy Agency are among the partnership clients, including Oak Ridge National Laboratory, with which the company has a contract. In 2016, VIE and Evatran established a joint venture to address the demand from original equipment manufacturers producing electric vehicles for the Chinese market. In December 2016, the company demonstrated a functional 7.2 kW production plugless system that charged a BMWi3 with 254 mm of clearance. [3]

3. Methodology

The core of this work is the modelling of a wireless charging system via Simulink. Chapter 3 shows step by step the process of assembling an ideal system as close as possible to the reality that can be later included in the road simulations.

1.18 Tools of the study

The “incipit” of this study is [41], which explores the boundaries of the wireless charging systems for electric vehicles by software simulations, with the aim of figuring out if systems like these could match the necessities of electric vehicles.

The main tools used in [41] are:

- **GOOGLE API**, to collect data about road trips in order to generate “drive cycles”. A drive cycle is the transcription of a road trip in numbers. It explains second by second the position, the speed, the road grade and many other fundamental information (the same that Google Maps shows during a common navigation with a smartphone).
- **EXCEL**, to sort data.
- **MATLAB/SIMULINK**, to create matrices that the model could use and to run it in Simulink in order to simulate different scenarios.

The main difference between this study and the previous one is the different approach, less mechanical and more electrical in this case. The main target of [41] is trying to understand if WPT systems could fit in an urban context, considering the traffic and the average speed.

1.19 Structure of the model

The model can be resumed in 5 essential blocks, as in Figure 3.1.

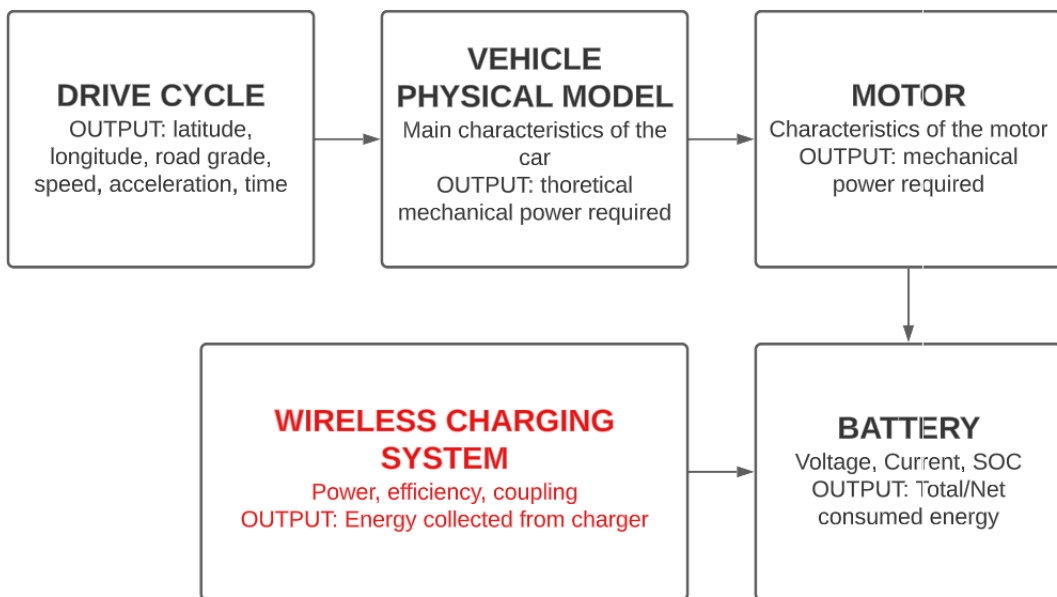


FIGURE 3.1 - SCHEME OF THE MODEL

DRIVE CYCLE: every simulation needs a scenario to take place. Through a GOOGLE API request it is possible to collect all the second-by-second geographical information about a chosen route that are sorted in matrices and stored in the drive cycle block. In particular the most important information are the latitude and longitude, the travelled distance, the average and instantaneous speed, the speed limits, the expected stops, the road grade, the acceleration. The information is the same that Google Maps uses during a navigation with our device.

It is fundamental to define the possible location of the wireless charging system, hence some parameters as:

- Speed limit = 50 [km/h]
- Road grade < 3%
- High density of stop signs, zebra crossings, intersections
- 30 meters before and after the traffic lights

An example of the drive cycle information is shown below in Figure 3.2. The first plot shows the speed, the second the acceleration, the third the road grade and the last one the activation/deactivation of the wireless charging system. In particular the “1” values represent an “ON” situation, while the “0” an “OFF”.

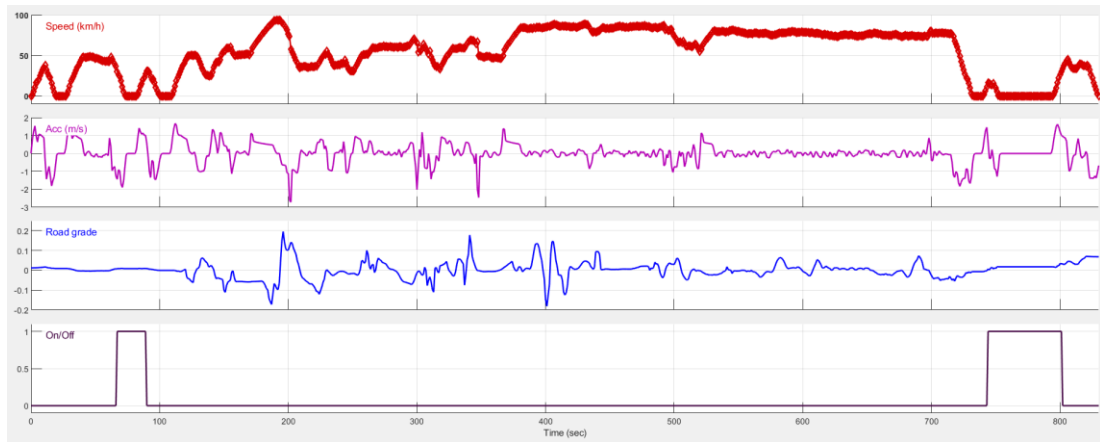


FIGURE 3.2 -- EXAMPLE OF DRIVE CYCLE

VEHICLE PHYSICAL MODEL: it uses as inputs the data coming from the drive cycle block to combine them with the vehicle physical parameters of different type of vehicles, such as weight, drag coefficient, size, and pressure of the tires, in order to calculate the “theoretical” mechanical power required to complete the route compensating all the different resistances (rolling, air, inertia). By modifying the parameters, it is possible to simulate different type of electric vehicle.

MOTOR: it contains all the information about the performance of the motor of the vehicle. For instance, it takes in account the efficiency, the rotations per minute, the gear selected. This is important in order to estimate the mechanical energy required for a specific drive cycle and vehicle. This block receives as inputs the mechanical power required (output of the vehicle physical model block) and simulates a working electrical motor to calculate the mechanical power required.

BATTERY: it models the battery of the vehicle with its capacity, state of charge, charging voltage and current. It uses the outputs from the motor block and from the wireless charging system in order to estimate the energy consumption, which represents the most important information.

WIRELESS CHARGING SYSTEM: the output is the energy delivered by the system during the trip. It will be examined in detail in section 3.3.

1.20 Wireless charging system

The modelling of our WPT system started considering a classic scheme, shown in Figure 3.3.

The reference for all the assumptions is [28].

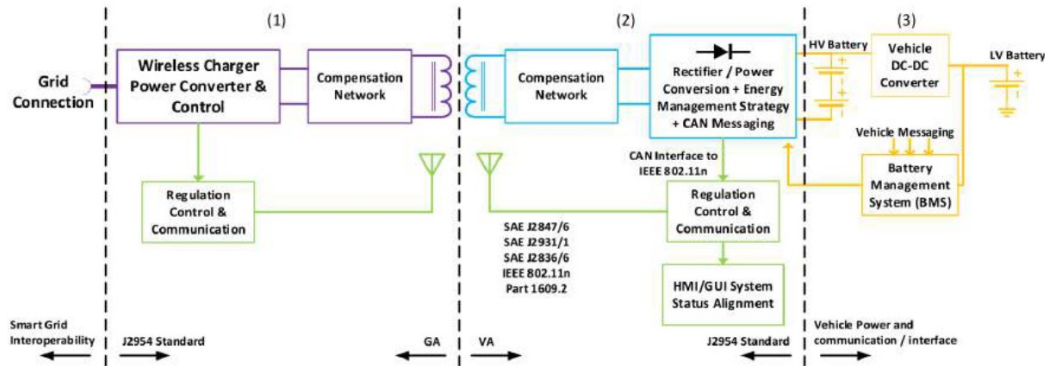


FIGURE 3.3 - TYPICAL FUNCTIONAL ELEMENTS OF A WIRELESS CHARGING SYSTEM (SOURCE [28])

To reduce the complexity of the model, some simplifications were assumed:

- perfect compensation on both the transmitting and receiving side, in order to assume the reactive power of the system equal to zero (Power Factor = 1). The assumption is realistic because [28] imposes PFs higher than 0.95 that can be achieved with different compensation networks.
- the control of the static converters is neglected.
- the filtering system is neglected.
- the power efficiency of all the static converters is assumed equal to 98%.
- the control of the charging power is achieved on the primary side
- constant vehicle-ground coils distance
- the interaction between only one transmitting coil and the receiving is considered
-

Figure 3.4 shows the block diagram of the wireless charging section, which is divided in 3 parts:

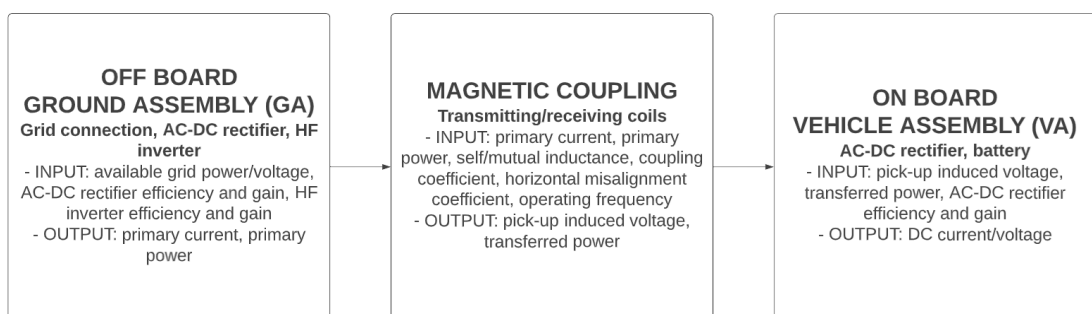


FIGURE 3.4 - WIRELESS CHARGING SYSTEM PARTS

- OFF BOARD: this part contains the grid connection and the static converters that feed the transmitting coil and regulate the power
- COUPLING SYSTEM: it models the transmitting/receiving coils and the magnetic induction effect between them
- ON BOARD: it contains the vehicle assembly (VA) with all the static converters that compose the on-board charger

1.1.1 Off-board – Ground assembly (GA)

Figure 3.5 shows the off-board part of the charging system.

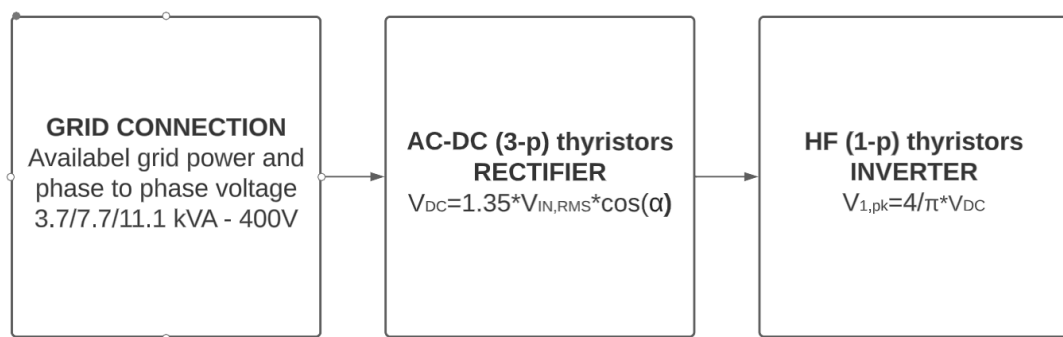


FIGURE 3.5 - OFF-BOARD SECTION OF WCS

The first step is the connection to the grid. The most common AC charging columns in the market usually have two AC plugs that can charge simultaneously two vehicles at the maximum power of 22kW. They each use a three-phase connection (Low voltage - 400V) with a maximum current of 32A. This kind of charging is part of the Mode 3 of IEC standard 61851 [9].

The three-phase active power (P_g) required to the grid is calculated as:

$$P_g [\text{kVA}] = 3 \cdot V_{LN,RMS} \cdot I_{RMS} = \sqrt{3} \cdot V_{LL,RMS} \cdot I_{RMS} \quad (3.1)$$

with $V_{LN,RMS}$, root-mean-square value of the line-to-neutral grid voltage, $V_{LL,RMS}$, root-mean-square value of the line-to-line grid voltage and I_{RMS} , the root-mean-square value of the required grid current.

Considering that systems like these are mainly intended for urban applications where low and medium voltage are more widespread, an upper limit of 11.1 kVA may seem feasible for

the grid to not overload it. On the other hand, this represents just a “hypothetical maximum” because in most cases the charging power limit is actually imposed by the on-board charger of the vehicle.

The majority of the on-board chargers of EVs in the market have the following limits:

- Single phase charging: 3.7 kW (16 A) or 7.4 kW (32 A)
- Three-phase charging: 11.1 kW (16A) or 22.2 kW (32 A)

These limits are given by the need of the manufacturers to increase the performance of the vehicles. Firstly, reducing the size of the converters (the higher the power the higher the size) and, consequently, reducing the weight on board. For the same reasons the DC high-power charging process requires an external charger in the column [9].

Due to the single-phase nature of the wireless charging system, we are modelling, we must consider the input-power limit of 7.4 kW of the on-board charger.

The standard [28] defines different ranges based on the maximum volt-amps drawn from the grid connection as shown in Table 3.1.

	WPT1	WPT2	WPT3	WPT4*	WPT5*
Range of Input Volt-Amps [kVA]	0 to 3.7	0 to 7.7	0 to 11.1	0 to 22	0 to 60

TABLE 3.1 - SAE J2954 WPT POWER CLASSIFICATIONS (*STILL UNDER STUDY) (SOURCE: [28])

Considering that the upper limit of the on board-charger is 7.4 kW and that we are neglecting the reactive power of the system, it is reasonable to select WPT3 (the maximum available for now) as the reference standard.

Another important characteristic of the system is its distribution along the road, under the pavement. The “concentrated” system, for instance, uses different coils hidden in the asphalt that are activated just when the vehicle is in correspondence. (Figure 3.6).

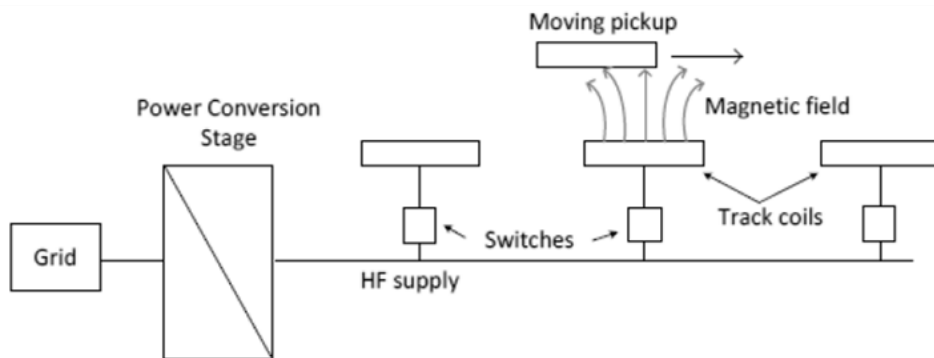


FIGURE 3.6 - CONCENTRATED WPT SYSTEM CONFIGURATION (SOURCE: [27])

The advantages of this configuration are the reduction of energy consumptions and of dispersed magnetic fields compared to a system with a single stretched coil. On the other hand, it is more expensive than the competitor.

To increase the frequency, it is fundamental to first rectify the alternate current/voltage coming from the grid. This is the aim of the single-phase thyristor rectifier.

The choice to introduce a phase-controlled rectifier is fundamental to vary the output voltage by modifying the triggering delay of the GTOs (Gate-Turn-Off) thyristors. It is important to have the chance to vary the output power in order to make the system adapt to the constantly changing load.

GTO thyristors match almost perfectly the voltage, current and frequency requirements of the wireless system. They have indeed good high-power performance in low frequency operation [42].

The average value of the output-direct voltage of a three-phase thyristor rectifier (V_{DC}) is given by:

$$V_{DC} [V] = 1.35 \cdot V_{LL,RMS} \cdot \cos(\alpha) \quad (3.2)$$

with V_{LL} , root-mean-square value of the line-to-line input voltage and α , phase-triggering delay of the thyristors.

The topology of a three-phase thyristor rectifier is shown in Figure 3.7.

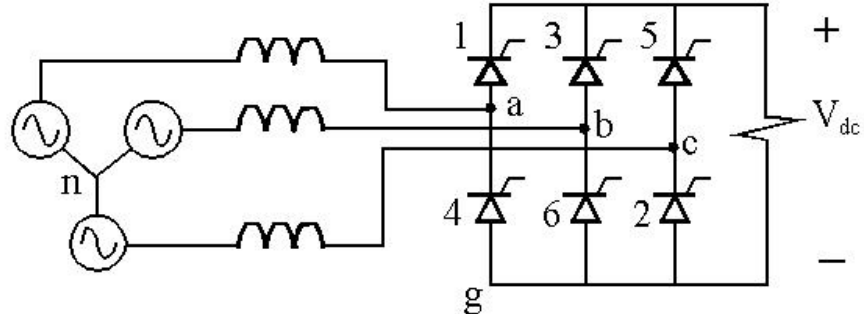


FIGURE 3.7 - THREE-PHASE THYRISTOR RECTIFIER (SOURCE: [43])

Once the voltage and current are rectified, a DC source is obtained.

The increase of the frequency from can be achieved by a high-frequency single-phase inverter composed of 4 MOSFETs (Metal-Oxide-Semiconductor Field Effect Transistors). The fast-switching characteristic is the main advantage of this solution [42]. The scheme is shown in Figure 3.8.

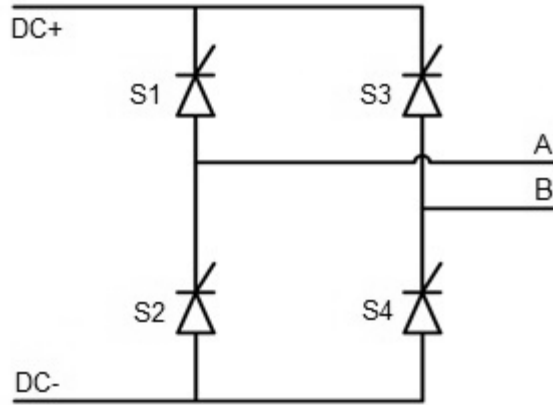


FIGURE 3.8 - FULL BRIDGE SINGLE-PHASE INVERTER (SOURCE: [43])

Increasing the frequency is an essential part of the process. As in a transformer, the higher the frequency the higher the inducting effect (as shown in Formula 3.3) and the lower the size of the system.

The induced voltage in the pick-up coil ($V_{p,pk}$) is given by [44]:

$$V_{p,pk} [V] = \omega \cdot M \cdot I_{t,pk} = 2 \cdot \pi \cdot f \cdot M \cdot I_{t,pk} \quad (3.3)$$

with $\omega = 2 \cdot \pi \cdot f$, pulsation of the system, f , operating frequency, M , mutual inductance of the coils and $I_{t,pk}$, peak value of the transmitting coil current.

The standard [28] uses 85 kHz as common operating frequency.

To obtain such a high frequency an appropriate inverter control technique must be established.

The Pulse Width Modulation technique would require a carrier signal with a too elevated frequency. An adequate technique could be the squared-wave one, for some reasons:

- It is possible to reduce the number of switching of the thyristors, so reducing the switching losses.
- It is possible to obtain the maximum value of the fundamental component of the alternate output voltage ($V_{1,pk}$) given by:

$$V_{1,pk} [V] = \frac{4}{\pi} \cdot V_{DC} \quad (3.4)$$

with V_{DC} , input direct voltage.

The main disadvantage of this solution is the fact that to regulate the output voltage it is necessary to regulate the input voltage. This requirement is obtained by the thyristor rectifier that precedes.

Another minor disadvantage is represented by the shape of the output voltage, not as sinusoidal as the one achieved with other techniques. Considering that the output alternate voltage is used for induction purpose by the transmitting coil and not directly used by an electronic device, this drawback is neglectable.

A resuming table of the assumed parameters is shown in Table 3.2.

GA/OFF-BOARD values	
P_g [kW]	3.7 – 7.7 – 11.1
V_{LL} [V]	400
3-p rectifier η [%]	98
1-p HF inverter η [%]	98

TABLE 3.2 - OFF BOARD VALUES OF THE MODEL

1.1.2 Mutual coupling (M)

The heart of the wireless process is the coupling effect between the transmitting and receiving coil. The better the coupling the higher the efficiency of the system.

One important parameter that influences the power transfer is the distance between the coils, the so-called “air gap”.

The standard [28] defines three classes of VA Coil Ground Clearance Range, as shown in Table 3.3.

Z-class	VA Coil Ground Clearance Range (mm)
Z1	100 to 150
Z2	140 to 210
Z3	170 to 250

TABLE 3.3 - SPECIFICATION OF THE SAE J2954 VA Z-CLASSES (SOURCE: [28])

Choosing the Z2 class it is possible to include a huge number of commercial vehicles (170 millimeters for KIA EV6 and Nissan Leaf for example).

Once fixed the class it is possible to obtain the mechanical parameters of the DD coils of a WPT3/Z2 system, summarized in Table 3.4. For the receiving coil (VA) and Table 3.5 for the transmitting one (GA).

	Coil + Ferrite Only	Housing
--	---------------------	---------

L x W x H [mm]	419 x 260 x 14.3	438 x 302 x 20
----------------	------------------	----------------

TABLE 3.4 - MECHANICAL DIMENSIONS OF THE PRODUCT VA WPT3/Z2 (SOURCE: [28])

	Coil + Ferrite Only	Housing
L x W x H [mm]	630 x 590 x 22	657 x 670 x 65

TABLE 3.5 -- MECHANICAL DIMENSIONS OF THE PRODUCT GA WPT3 (SOURCE: [28])

The values of the self-inductances (L) (Table 3.6 and Table 3.7) and of the coupling coefficient (k) (Table 3.8) of a WPT3 system are resumed in the standard [28] too:

L_{VA_min} [μH]	44.7
L_{VA_max} [μH]	48.2

TABLE 3.6 - VA COIL INDUCTANCE (SOURCE: [28])

L_{GA_min} [μH]	62.5
L_{GA_max} [μH]	65.8

TABLE 3.7 - GA COIL INDUCTANCE (SOURCE: [28])

k_{min}	0.134
k_{max}	0.318

TABLE 3.8 - COUPLING K BETWEEN GA AND VA COIL FOR Z2 CLASS (SOURCE: [28])

For our simulations we assumed the max values for each parameter, adapting them later to the different charging conditions. Hence:

L_{VA} [μH]	48.2
L_{GA} [μH]	65.8
k	0.318

TABLE 3.9 - ASSUMPTIONS FOR THE MODEL (SOURCE: [28])

The configuration of the coils is shown in Figure 3.9, in which the orange part represents the active coil while the grey one represents the ferrite core aimed to contain the magnetic field.

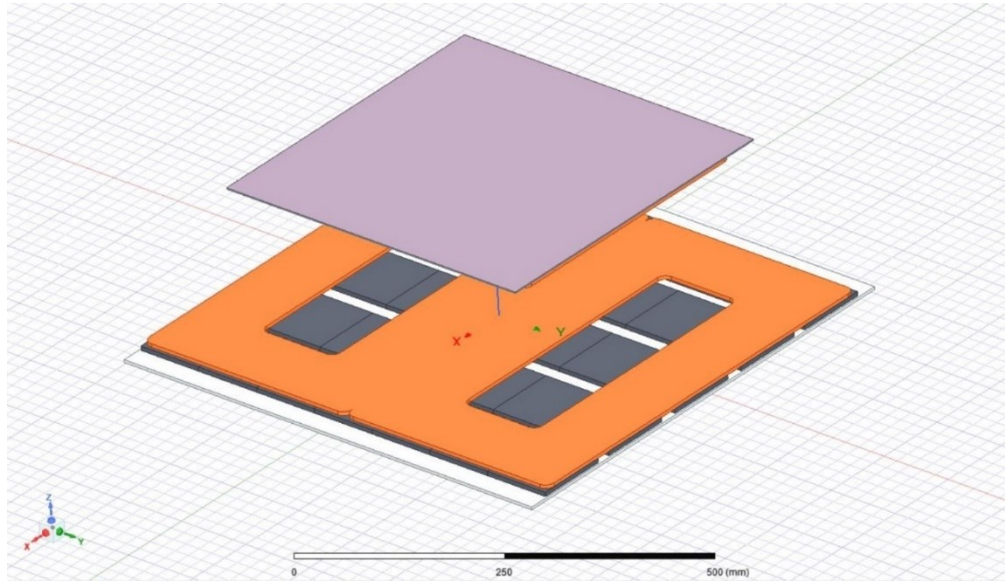


FIGURE 3.9 - CONFIGURATION OF THE COILS

With the available values it is possible to calculate the maximum value (M_0) of the mutual inductance between the coils [3]:

$$M_0 [H] = k_{max} \cdot \sqrt{L_{GA} \cdot L_{VA}} \quad (3.5)$$

With the aforementioned values, M_0 is equal to $M_0 = 1.8 \cdot 10^{-5} H$.

As shown in Formula 3.3, M is an indicator of the quality of the coupling. The higher the M , the better the coupling, the higher the power transmitted. In dynamic systems the mutual inductance varies continuously because of the always changing relative position of the coils, both in the direction of the movement (longitudinal) and horizontally. This gap from the perfect alignment is called “misalignment” and represents a crucial factor for the dynamic-charging process.

The longitudinal misalignment is the effect of the movement of the pick-up coil on the vehicle in the direction of movement. The typical shape is shown in Figure 3.10.

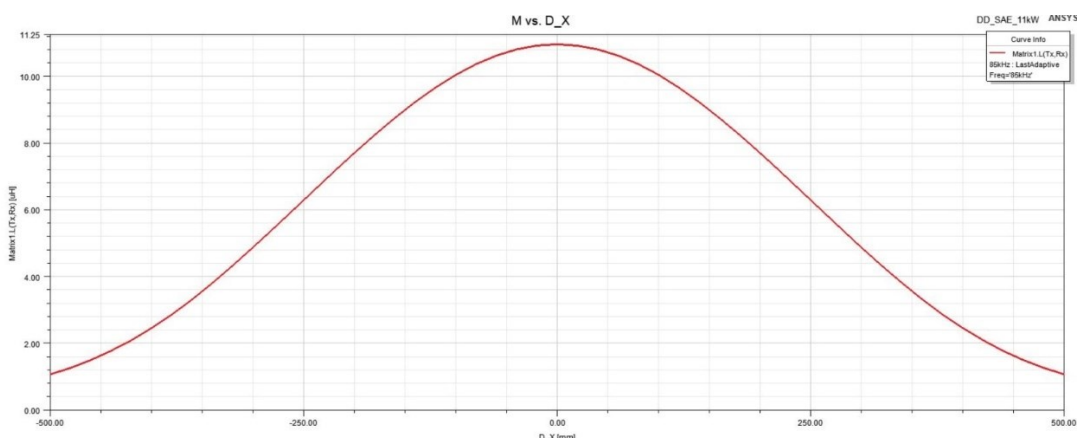


FIGURE 3.10 - TYPICAL SHAPE OF M WITH LONGITUDINAL MISALIGNMENT

From the information of the plot, M increases along the x-direction from a minimum to a maximum value M_0 when the coils are perfectly aligned.

With a WPT concentrated system in which the ground coils are one close to the other (similar to a stretched-track system) it would be possible to keep the M value almost constant and almost equal to a value close to the maximum one. Increasing the longitudinal distance between the transmitting coils the average M along the track decreases proportionally.

To consider this effect a track coverage ratio coefficient (ε) to be applied to the output power, is considered:

$$\varepsilon = \frac{X_t}{D + X_t} \quad (3.6)$$

with X_t , length of the tracking coil (650mm) and D , longitudinal distance between two consecutive tracking coils.

To simplify the discussion, we assumed a minimum longitudinal distance between the tracking coils equal to the size of the pick-up coil (420mm) in order to consider a situation in which just one transmitting coil at the time is activated and hence the interaction between just one transmitting coil and the receiving one is studied.

D [mm]	ε
420	0.6075
470	0.5804
520	0.5556
570	0.5328
620	0.5118
670	0.4924
720	0.4745

TABLE 3.10 - ε vs. D

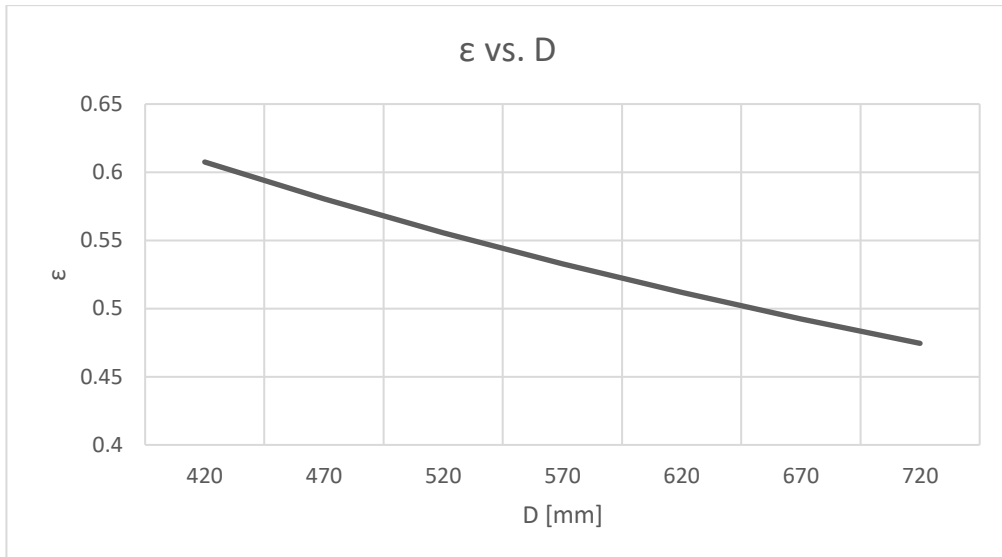


FIGURE 3.11 - ϵ vs. D

Because of the always changing position of the car, a horizontal displacement (y-direction) between the coils must be taken in account. Even though with the autonomous driving it is going to be easier to obtain a good alignment with the charging system, a variation in the mutual inductance value must be considered.

By a FEM analysis of the mutual coupling of the coils executed by Prof. Alicia Triviño-Cabrera from the University of Málaga, it was possible to obtain the plot of $\frac{M}{M_0}$ for different y-offsets (Figure 3.12). The positive values of y-offset represent a “right” misalignment, hence the pick-up coil is on the right of the centred position (0, perfect alignment). The negative values represent a “left” misalignment. The particular shape of the plot with two minimums at about 20 cm of displacement both in the left and right direction is given by the shape of the DD coils. When the “junction” of the pick-up rectangular sub-coils is in correspondence of the center one of the sub-coils of the transmitting coil, a minimum appears.

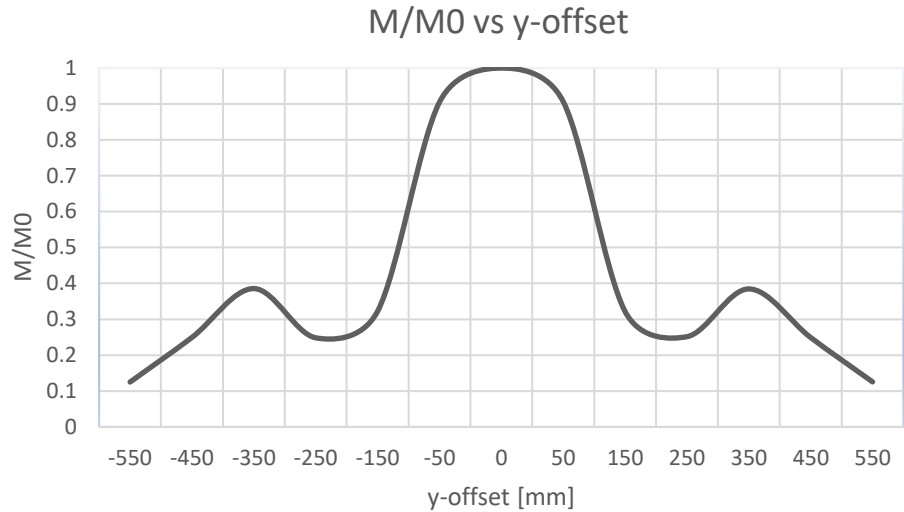


FIGURE 3.12 - M/M₀ VS. Y-OFFSET FOR DD COILS

Once established the offset, the K_y coefficient to consider the lateral misalignment is deduced by the following plot which represents the zoom of one of the two specular parts of Figure 3.12. It is indeed right to say that K_y is proportional to $\frac{M}{M_0}$.

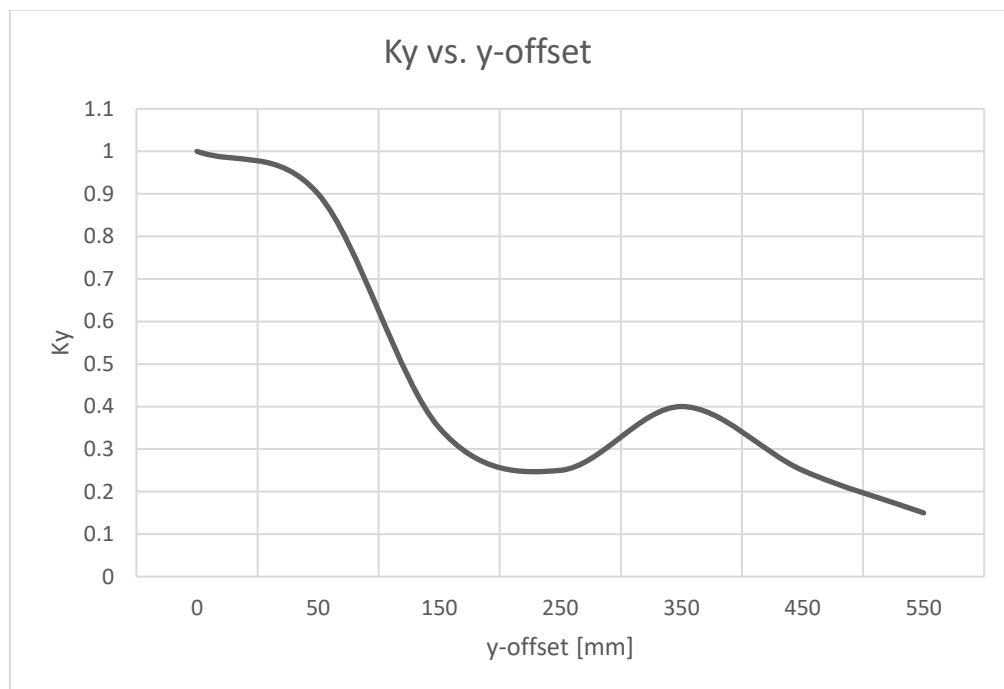


FIGURE 3.13 - K_y VS. Y-OFFSET

The final value of the mutual coupling (M) is calculated as it follows, taking in account both the ε and the K_y coefficient:

$$M = M_0 \cdot \varepsilon \cdot K_y \quad (3.7)$$

A resuming table of the assumed parameters is shown in Table 3.11.

MUTUAL COUPLING values	
Z2 air gap [mm]	140 to 210
VA coil size: L x W x H [mm]	419 x 260 x 14.3
L _{VA} [μ H]	48.2
GA coil size: L x W x H [mm]	630 x 590 x 22
L _{GA} [μ H]	65.8
k	0.318
M ₀ [μ H]	18
Minimum D [mm]	420
K _y	Figure 3.13

TABLE 3.11 - MUTUAL COUPLING VALUES OF THE MODEL

1.1.3 On-board - Vehicle assembly (VA)

The on-board components of the system are reduced to two, thanks to the primary side power control. (Figure 3.14)

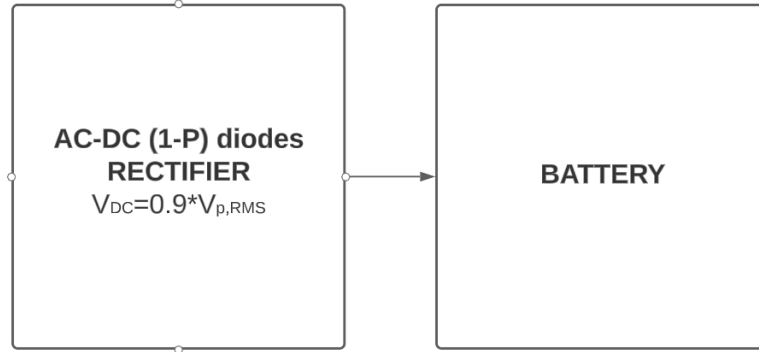


FIGURE 3.14 - ON-BOARD SECTION OF WCS

The induced voltage (V_p) on the pick-up coil is given by Formula 3.3. The pick-up current (I_p) is hence, from [45]:

$$I_p [A] = \frac{V_p}{R_L} \quad (3.5)$$

with R_L , battery resistance given by

$$R_L [\Omega] = \frac{V_{bat}^2}{P_c} \quad (3.6)$$

with V_{bat} , nominal voltage of the battery and P_c , expected charging power.

It is well known that batteries need constant voltage or current to complete the charging process. Because of the continuously changing conditions that characterize the dynamic wireless system it is fundamental to design a flexible system. At the same time, the choice of regulating the power on the primary side of the system largely simplifies the secondary topology.

To rectify the voltage induced in the pick-up coil a single-phase non-controllable diode rectifier is the simplest solution (Figure 3.15).

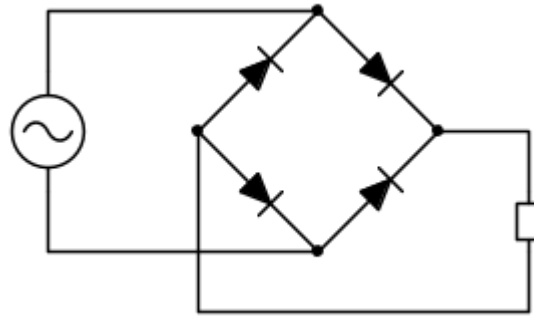


FIGURE 3.15 - SINGLE-PHASE DIODE RECTIFIER (SOURCE: [46])

The output voltage is given by:

$$V_{DC} [V] = 0.9 \cdot V_{p,RMS} \quad (3.7)$$

With $V_{p,RMS}$, root mean square value of the induced voltage on the pick-up coils.

A DC-DC conditioning stage could also be considered. In this model, thanks to the primary-side power regulation, it is possible to neglect it.

The standard [28] defines 280-420V as range for the charging voltage and, as stated in [47], the majority of the EVs fit in this range.

A resuming table of the assumed parameters is shown in Table 3.12.

VA/ON-BOARD values	
1-p rectifier η [%]	98

TABLE 3.12 - VA/ON-BOARD VALUES OF THE MODEL

1.21 Power, energy, overall efficiency

The power and the energy transferred by the system can be calculated using Formula 3.3.

The induced voltage is composed by two components: the first one given by the inductive effect (as a transformer) and the second one given by the motion effect. The second one, as shown in [45] can be neglected.

From Formula (3.3) the average transferred power (P_L) to R_L can be calculated as:

$$P_c [W] = \frac{1}{2} I_p^2 R_L = \frac{1}{2} \frac{(\omega \cdot M \cdot I_t)^2}{R_L} \quad (3.8)$$

By integrating this value for the time (T_X) that takes for the vehicle to cover the length (X) of the ground coil at the average speed (U_{avg}), we obtain the transferred energy (E):

$$E [J] = \int_0^{T_X} P_c(t) dt \quad (3.9)$$

with $dt = \frac{1}{U} dx$.

Formula (3.9) can be rewritten as:

$$E [J] = \frac{1}{U_{avg}} \int_{x(0)}^{x(0)+X} P_c(t) dx \quad (3.10)$$

and with (3.8), (3.10) becomes:

$$E [J] = \frac{1}{U_{avg}} K \int_{x(0)}^{x(0)+X} M_{(x)}^2 dx \quad (3.11)$$

with $K = \frac{1}{2} \frac{(\omega \cdot I_t)^2}{R_L}$.

Formula (3.11) shows that the transferred energy is inversely proportional to the speed.

This is not given by the higher/lower quality of the power transfer at high speed (as aforementioned the “motion” effect is neglectable in the calculation of the induced voltage).

The higher the speed, the lower the time spent on the charging system, the lower the energy transferred. Theoretically, the more “static” the charging process is, the better it is.

Another parameter that influences the transferred power is ε . Increasing the number of the coils leads to an increase of the energy transferred.

The target of the model is to reach the highest WPT3 acceptable efficiency for the standard [28], shown in Table 3.13. The efficiency considers the overall process, from the grid to the battery.

WPT class	At centred position	In alignment tolerance area
WPT1	80%	75%
WPT2	82%	77%
WPT3	85%	80%

TABLE 3.13 - MINIMUM SYSTEM EFFICIENCY REQUIREMENTS (SOURCE: [28])

The vehicle used in the simulations is the KIA EV6 Air whose main characteristics are shown in the following table.



FIGURE 3.16 - KIA EV6 AIR (SOURCE: [49])

PARAMETER	VALUE
Battery capacity [kWh]	58
Battery nominal voltage [V]	360
Power [HP]/[kW]	167/124
Weight [kg]	1860
0-100 km/h [s]	8.5
Maximum speed [km/h]	185
WLTP range [km]	400

TABLE 3.14 - KIA EV6 AIR CHARACTERISTICS (SOURCE: [49])

1.22 Scenarios

The first scenario is an urban trip in Lisbon downtown. The main details of the drive cycle, obtained by Google API, are resumed in Table 3.15.

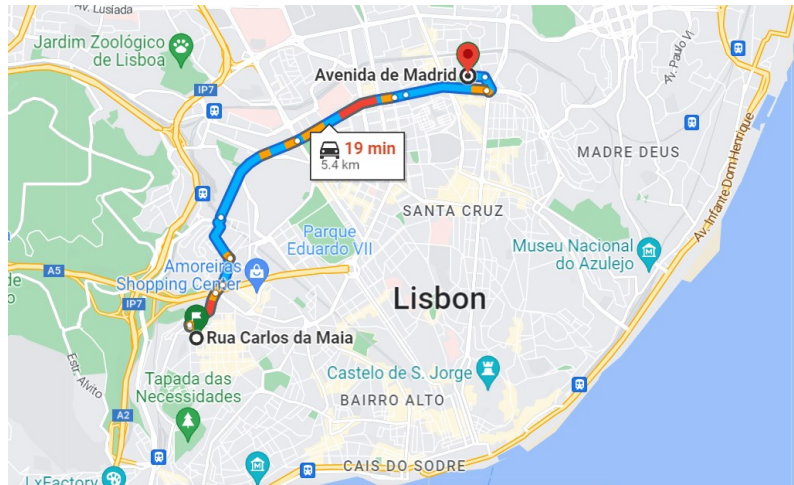


FIGURE 3.17 - RUA CARLOS DA MAIA-AVENIDA DE MADRID (SOURCE: [50])

PARAMETER of the journey	VALUE
Rua Carlos da Maia-Avenida de Madrid	
Charging system	3.7 kW, $K_y=1$, $\varepsilon=0.6075$
Length of the journey [km]	5.4
Estimated U_{avg} [km/h]	18
Estimated journey time [']	18

TABLE 3.15 - INFORMATION ABOUT THE JOURNEY RUA CARLOS DA MAIA-AVENIDA DE MADRID IN LISBON (SOURCE: [50])

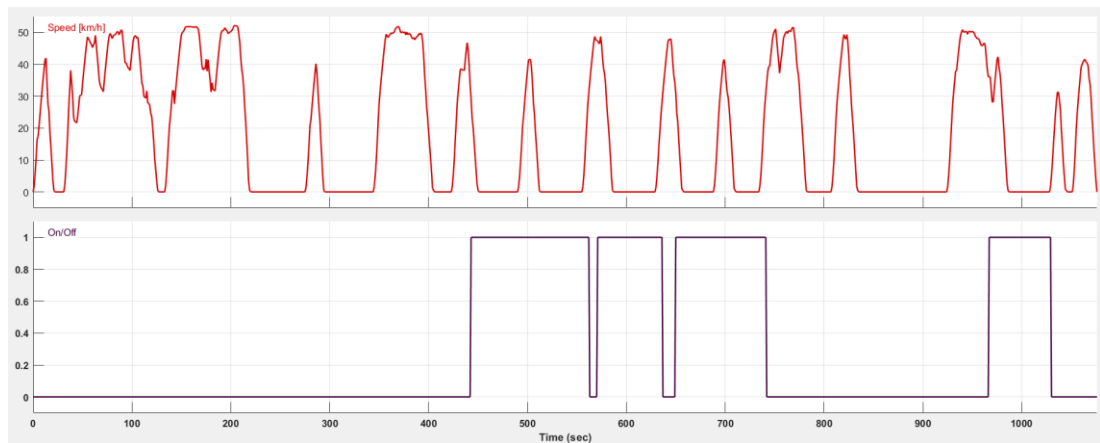


FIGURE 3.18 - SPEED PROFILE OF THE FIRST JOURNEY AND WCS ACTIVATION

The second-simulated scenario is a sub-urban trip in the metropolitan area of Lisbon.

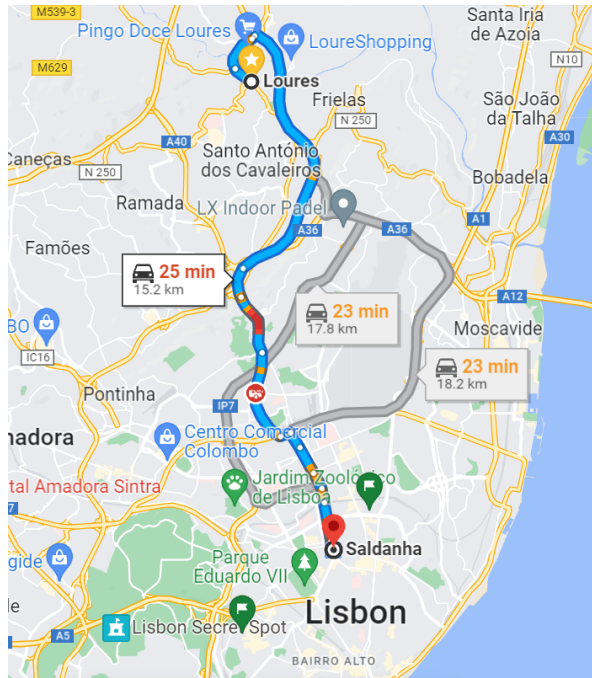


FIGURE 3.19 - SALDANHA (LISBON) – LOURES (SOURCE: [50])

PARAMETER of the journey	VALUE
Saldanha (Lisbon) – Loures	
Charging system	3.7 kW , $K_y=1$, $\varepsilon=0.6075$
Length of the journey [km]	15.2
Estimated U_{avg} [km/h]	38
Estimated journey time [']	25

TABLE 3.16 – INFORMATION ABOUT THE JOURNEY SALDANHA (LISBON) – LOURES (SOURCE: [50])

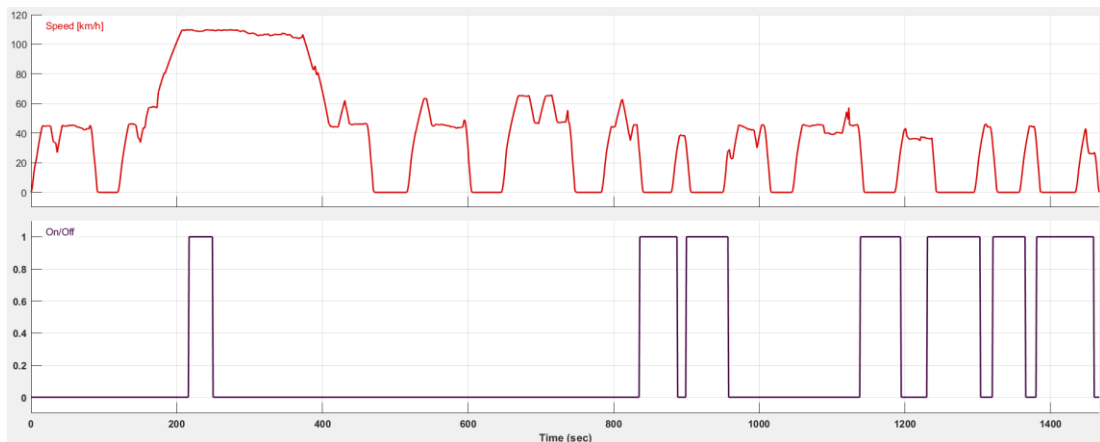


FIGURE 3.20 - SPEED PROFILE OF THE SECOND JOURNEY AND WCS ACTIVATION

The third simulated scenario is another sub-urban trip with higher average speed.

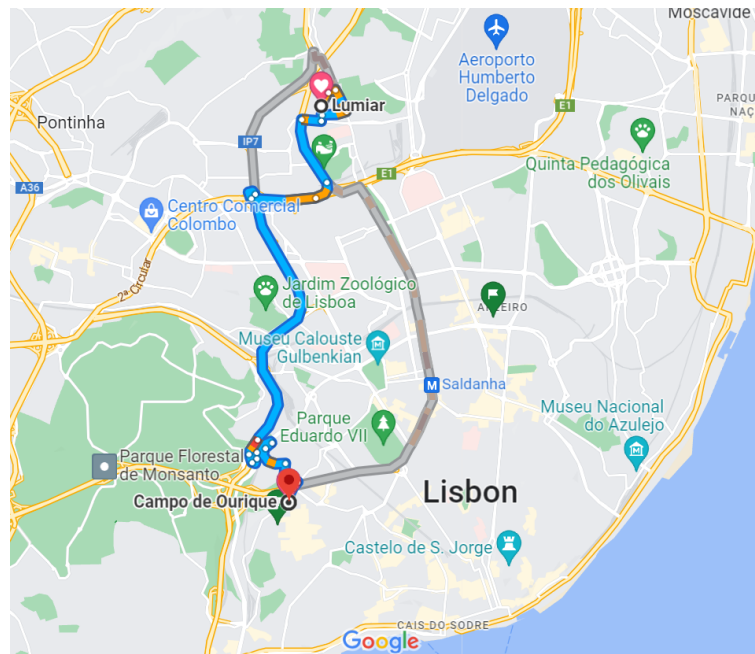


FIGURE 3.21 - LUMIAR - CAMPO DE OURIQUE (SOURCE: [50])

PARAMETER of the journey	VALUE
Lumiar – Campo de Ourique	
Charging system	$3.7 \text{ kW}, K_y=1, \epsilon=0.6075$
Length of the journey [km]	9.4
Estimated U_{avg} [km/h]	45
Estimated journey time [']	13

TABLE 3.17 - INFORMATION ABOUT THE JOURNEY LUMIAR – CAMPO DE OURIQUE (SOURCE: [50])

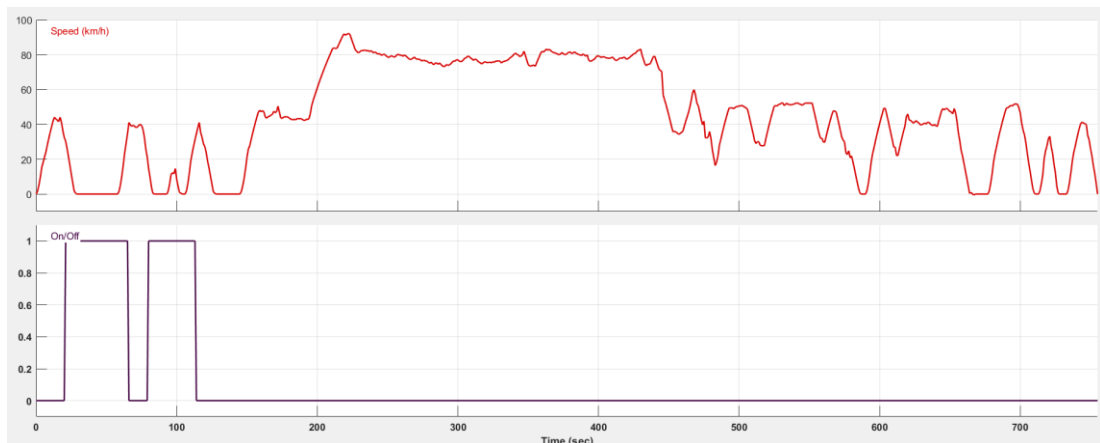


FIGURE 3.22 - SPEED PROFILE OF THE THIRD JOURNEY AND WCS ACTIVATION

4. Results

The “incipit” of this chapter is the fundamental verification of the model through the literature. After this step different scenarios are simulated. The target is to test the system in different conditions in order to figure out where it fits better and which parameters affect more the process.

1.23 Validation of the model

To verify the model, two low-power examples from the literature are used.

The first one, shown in [3], is a WPT system designed to feed a 300V battery with 3.7 kW (WPT1) / Z2-class. The structure of the charging system is similar to the one of the model, with power control on the primary side to simplify the complexity and the weight on the secondary side.

Inputs and outputs of the example [3] are resumed here in Table 4.1.

PARAMETER	VALUE
P_g [W]	3820
V_{LL} [V]	400
L_1 [μ H]	475
L_2 [μ H]	152
M [μ H]	37
k	0.1377
f [kHz]	85
P_t [W]	3750
$I_{t,RMS}$ [A]	13.78
R_L [Ω]	25
V_{DC} [V]	300
I_{DC} [A]	12.16
P_c [W]	3700
η	0.969

TABLE 4.1 - INPUTS AND OUTPUTS OF EXAMPLE [3]

The outputs obtained by running a simulation with the values of Table 4.1 with the model are summarised in Table 4.2.

PARAMETER	VALUE
P_g [W]	3820
V_{LL} [V]	400
Three-phase rectifier triggering delay $\cos(\alpha)$	0.465
L_1 [μH]	475
L_2 [μH]	152
M [μH]	37
k	0.1377
f [kHz]	85
P_t [W]	3669
$I_{t,RMS}$ [A]	22.95
R_L [Ω]	25
V_{DC} [V]	288.5
I_{DC} [A]	12.56
P_c [W]	3624
η	0.949

TABLE 4.2 - INPUTS AND OUTPUTS OF THE MODEL

From a comparison between the two tables, the deviations of the values obtained by the model are:

PARAMETER	LITERATURE [3]	MODEL	DEVIATION [%]
$I_{t,RMS}$ [A]	13.78	22.95	+67
V_{DC} [V]	300	288.5	-4
I_{DC} [A]	12.16	12.56	+3
P_c [W]	3700	3624	-2
η	0.969	0.949	-2

TABLE 4.3 - DEVIATIONS FROM EXAMPLE [3]

It is possible to notice that the value of the primary current is quite different. This is given by the structure of the model that requires a high value of current in the transmitting coil to

increase the power transfer, as shown in Formula (3.3). The other values confirm the reliability of the model.

The second example [48], is a DWCS designed to transfer 3kW of power to an 80V battery. The target of the system is charging the battery of a light-duty vehicle by means of identical transmitting and receiving coils.

Inputs and outputs of the example [48] are resumed here in Table 4.4.

PARAMETER	VALUE
P_g [W]	4126
V_{LL} [V]	400
L1 [μ H]	54.7
L2 [μ H]	54.7
M [μ H]	15
k	0.27
f [kHz]	85
P_t [W]	3900
$I_{t,RMS}$ [A]	10.96
R_L [Ω]	3
V_{DC} [V]	80
I_{DC} [A]	37.5
P_c [W]	3000
η	0.73

TABLE 4.4 - INPUTS AND OUTPUTS OF EXAMPLE [48]

The outputs obtained by running a simulation with the values of Table 4.4 with our model are resumed in Table 4.5.

PARAMETER	VALUE
P_g [W]	4126
V_{LL} [V]	400
Three-phase rectifier triggering delay $\cos(\alpha)$	0.64
L1 [μ H]	54.7
L2 [μ H]	54.7

M [μ H]	15
k	0.27
f [kHz]	85
P _t [W]	3964
I _{t,RMS} [A]	18.01
R _L [Ω]	3
V _{DC} [V]	90.36
I _{DC} [A]	32.8
P _c [W]	2964
η	0.718

TABLE 4.5 - INPUTS AND OUTPUTS OF THE MODEL

PARAMETER	LITERATURE [48]	MODEL	DEVIATION [%]
I _{t,RMS} [A]	10.96	18.01	+64
V _{DC} [V]	80	90.36	+13
I _{DC} [A]	37.5	32.8	-14
P _c [W]	3000	2964	-1
η	0.73	0.718	-2

TABLE 4.6 – DEVIATION FROM EXAMPLE [48]

In this second case we observe the same deviation on the primary current, and a higher deviation on the rectified voltage and current on the secondary side. These deviations are generated by the difference between the structure of the system in the example and the model (no DC-DC conditioning rectifier in the model).

In Table 4.6 the parameters of the model with the SAE J2954 Standard inputs and an input power of 3.7 kW (WPT1), to charge a 360V battery obtaining the minimum acceptable efficiency (85%) for the standard.

PARAMETER	VALUE
P _g [W]	3700
V _{LL} [V]	400
Three-phase rectifier triggering delay $\cos(\alpha)$	0.18
L1 [μ H]	48.2

$L_2 [\mu\text{H}]$	65.8
$M [\mu\text{H}]$	18
k	0.318
$f [\text{kHz}]$	85
$P_t [W]$	3553
$I_{t,RMS} [A]$	40.61
$R_L [\Omega]$	42
$V_{DC} [V]$	349.4
$I_{DC} [A]$	9.058
$P_c [W]$	3164
η	0.855

TABLE 4.6 - INPUT AND OUTPUT VALUES OF THE MODEL (SAE J2954 PARAMETERS)

Like in the verification cases the main drawback of the model is given by the high value of current required on the primary side to obtain an acceptable power transfer.

1.24 Influence of average speed (U_{avg})

A resume of the different energy values of the first journey is here shown:

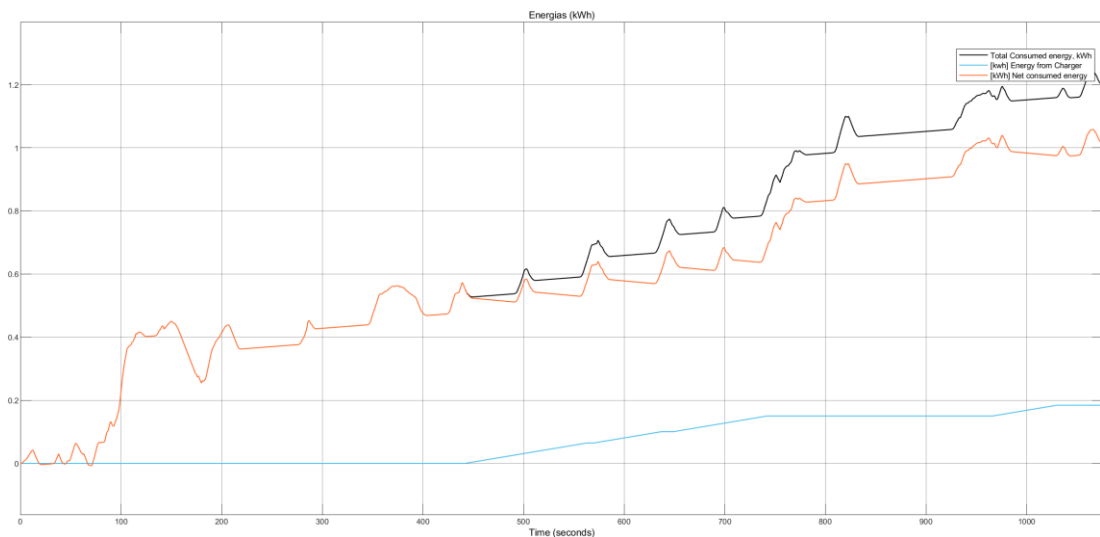


FIGURE 4.1 - TOTAL CONSUMED ENERGY (BLACK), ENERGY FROM CHARGER (BLUE) AND NET CONSUMED ENERGY (ORANGE) IN THE FIRST JOURNEY

Total consumed energy [kWh]	1.2
Energy from charger [kWh]	0.1842

Net consumed energy [kWh]	1.016
---------------------------	-------

TABLE 4.7 - RESUMING TABLE OF THE ENERGIES IN THE FIRST SIMULATION

The collected energy ratio (χ) between the energy from charger and the total consumed energy (relative contribution of the wireless charging system to the trip) is hence defined:

$$\chi_1 = \frac{\text{Energy from charger [kWh]}}{\text{Total consumed energy [kWh]}} = \frac{0.1842}{1.016} \approx 0.15$$

A resume of the different energy values of the second journey is here shown:

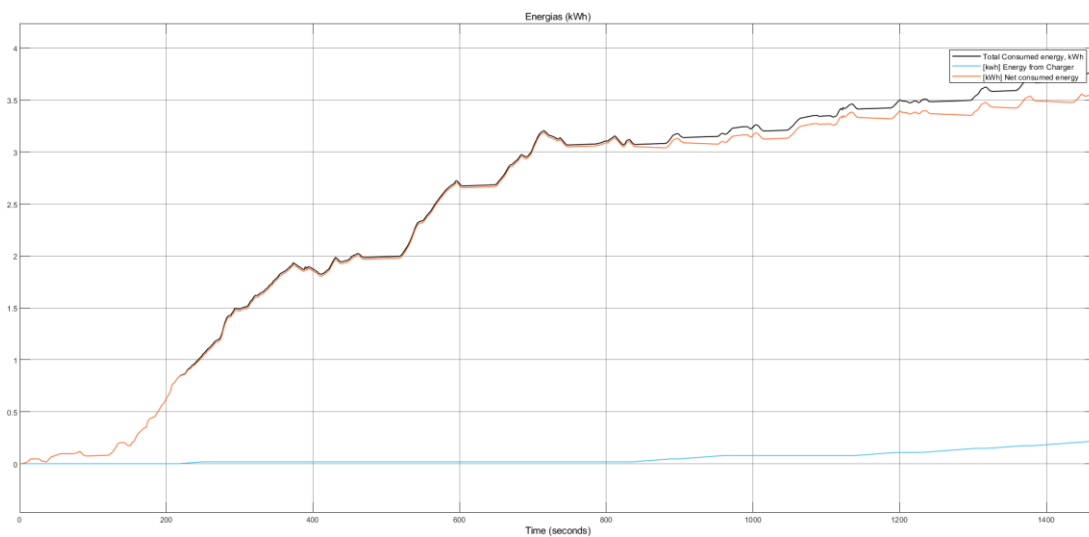


FIGURE 4.2 - TOTAL CONSUMED ENERGY (BLACK), ENERGY FROM CHARGER (BLUE) AND NET CONSUMED ENERGY (ORANGE) IN THE SECOND JOURNEY

Total consumed energy [kWh]	3.751
Energy from charger [kWh]	0.2152
Net consumed energy [kWh]	3.536

TABLE 4.8 - RESUMING TABLE OF THE ENERGIES IN THE SECOND SIMULATION

The χ ratio is given by:

$$\chi_2 = \frac{\text{Energy from charger [kWh]}}{\text{Total consumed energy [kWh]}} = \frac{0.2152}{3.751} \approx 0.06$$

A resume of the different energy values of the third journey is here shown:

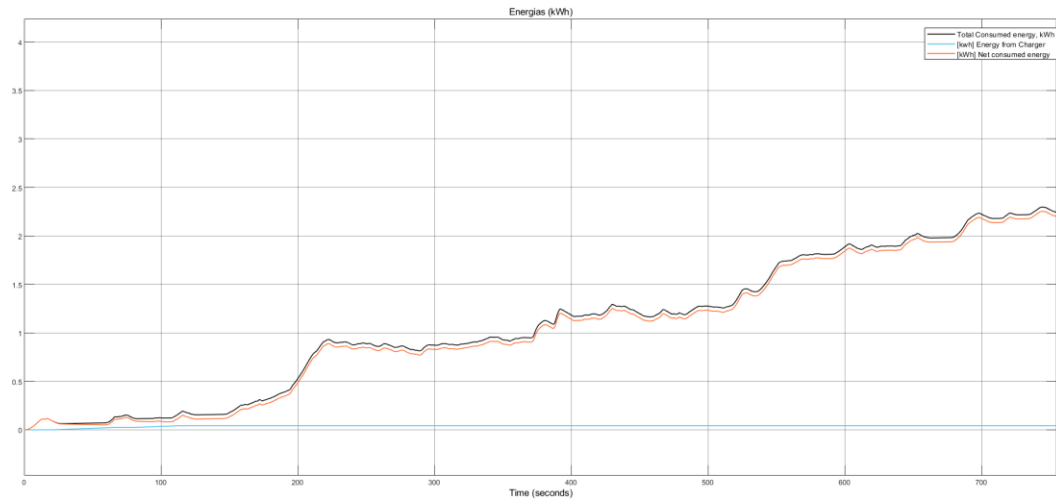


FIGURE 4.3 - TOTAL CONSUMED ENERGY (BLACK), ENERGY FROM CHARGER (BLUE) AND NET CONSUMED ENERGY (ORANGE) IN THE THIRD JOURNEY

Total consumed energy [kWh]	2.246
Energy from charger [kWh]	0.04325
Net consumed energy [kWh]	2.203

TABLE 4.9 - RESUMING TABLE OF THE ENERGIES IN THE SECOND SIMULATION

As in the other simulations, the χ ratio is so calculated:

$$\chi_3 = \frac{\text{Energy from charger [kWh]}}{\text{Total consumed energy [kWh]}} = \frac{0.04325}{2.246} \approx 0.02$$

A comparison between the χ ratio of the three different scenarios is shown here:

JOURNEY	U_{avg} [km/h]	χ [%]
Rua Carlos da Maia - Avenida de Madrid (Lisbon)	18	15
Saldanha (Lisbon) – Loures	38	6
Lumiar – Campo de Ourique	45	2

TABLE 4.10 - COMPARISON BETWEEN THE SIMULATIONS

Analysing the results obtained by the different kinds of journey it is possible to notice that the ratio χ ($= \frac{\text{Energy from charger [kWh]}}{\text{Total consumed energy [kWh]}}$) is higher for low speed journeys, as reported by Table 4.10. This effect can be explained considering Formula 3.11. The higher the average speed, the lower the time spent by the vehicle on the charging track and, consequently, the

lower the collected energy. Urban journeys have lower average speed because of the stops caused by traffic lights, roundabouts and crowded intersections.

1.25 Influence of available power (P_g)

Once shown that the influence of the average speed is a factor for DWCSs it is interesting to study the effect of the increase of the available power. The first trip is used as simulation scenario (Table 4.11).

Rua Carlos da Maia - Avenida de Madrid (Lisbon)		
PARAMETER	WPT2	WPT3
P_g [W]	7700	11100
V_{LL} [V]	400	400
Three-phase rectifier triggering delay $\cos(\alpha)$	0.36	0.54
L1 [μH]	48.2	48.2
L2 [μH]	65.8	65.8
M [μH]	18	18
k	0.318	0.318
f [kHz]	85	85
P_t [W]	7107	10066
$I_{t,RMS}$ [A]	40.61	40.61
R_L [Ω]	21	14
V_{DC} [V]	349.4	349.4
I_{DC} [A]	18.12	27.17
P_c [W]	6629	9493
ϵ	0.6075	0.6075
K_y	1	1
η	0.8552	0.8552
<hr/>		
Total consumed energy [kWh]	1.2	1.2
Energy from charger [kWh]	0.3684	0.5527
Net consumed energy [kWh]	0.8317	0.6475
<hr/>		

χ	$\frac{0.3684}{1.2} \approx 0.31$	$\frac{0.5527}{1.2} \approx 0.46$
--------	-----------------------------------	-----------------------------------

TABLE 4.11 - UPSCALED CHARGING SYSTEMS PARAMETERS, ENERGIES AND X

As shown in Table 4.12 increasing the available power from the grid it is possible to increase linearly the transferred energy.

P_g [kVA]	χ [%]
3.7 (WPT1)	15
7.7 (WPT2)	33
11.1 (WPT3)	46

TABLE 4.12 - DIFFERENT VALUES OF X FOR DIFFERENT AVAILABLE GRID POWERS (P_g)

The increase of the available power is reflected by a linear increase of the χ ratio that is an index of the contribution of the WCS to the trip.

1.26 Influence of track coverage ratio (ϵ)

To study the influence of the distance between the tracking coils, the following trip and charging system parameters are assumed.

Rua Carlos da Maia - Avenida de Madrid (Lisbon)			
Charging system: Table 4.11 (WPT3) - $K_y=1$			
Total consumed energy [kWh]: 1.2			
D [mm]	ϵ	Energy from charger [kWh]	χ
420	0.6075	0.5527	0.46
470	0.5804	0.5280	0.44
520	0.5556	0.5054	0.42
570	0.5328	0.4847	0.40
620	0.5118	0.4656	0.39
670	0.4924	0.4480	0.37
720	0.4745	0.4316	0.36
770	0.4577	0.4164	0.35

TABLE 4.13 -- DIFFERENT ϵ FOR DIFFERENT D

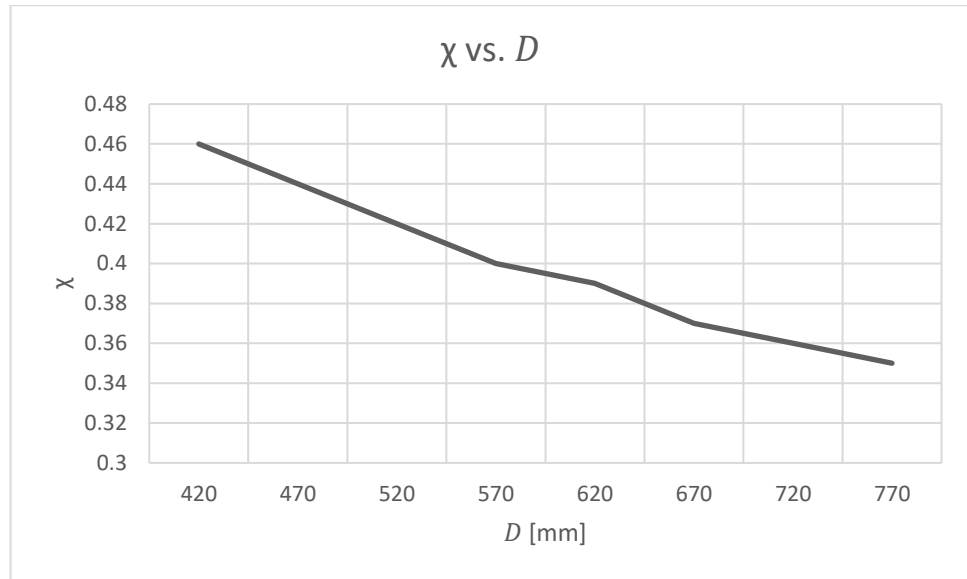


FIGURE 4.4 - χ vs. D

As shown in Figure 4.4 the closer the tracking coils are, the higher the energy transferred. Increasing the density of transmitting coils allows indeed for more interactions between the magnetic fields of the tracking ad receiving coils. For instance, by reducing D from 72cm to 42 cm provides an increase of 22% of transferred energy.

1.27 Influence of Horizontal misalignment (K_y)

Applying the K_y coefficient, the M value is no longer equal to the maximum value M_0 , but decreases because of the misalignment. The effect of a constant-horizontal misalignment throughout all the trip is shown in Table 4.14.

Rua Carlos da Maia - Avenida de Madrid (Lisbon)				
Charging system: Table 4.11 (WPT3) – $\varepsilon=0.6075$				
Total consumed energy [kWh]: 1.2				
y-OFFSET [mm]	K_y	M [μ H]	Energy from charger [kWh]	χ
0	1	18	0.5527	0.46
50	0.9	16	0.4477	0.37
150	0.35	6.3	0.0677	0.06
250	0.25	4.5	0.03454	0.03
350	0.4	7.2	0.08843	0.07
450	0.25	4.5	0.03454	0.03
550	0.15	2.7	0.01243	0.01

TABLE 4.14 - KY EFFECT ON ENERGY TRANSFER

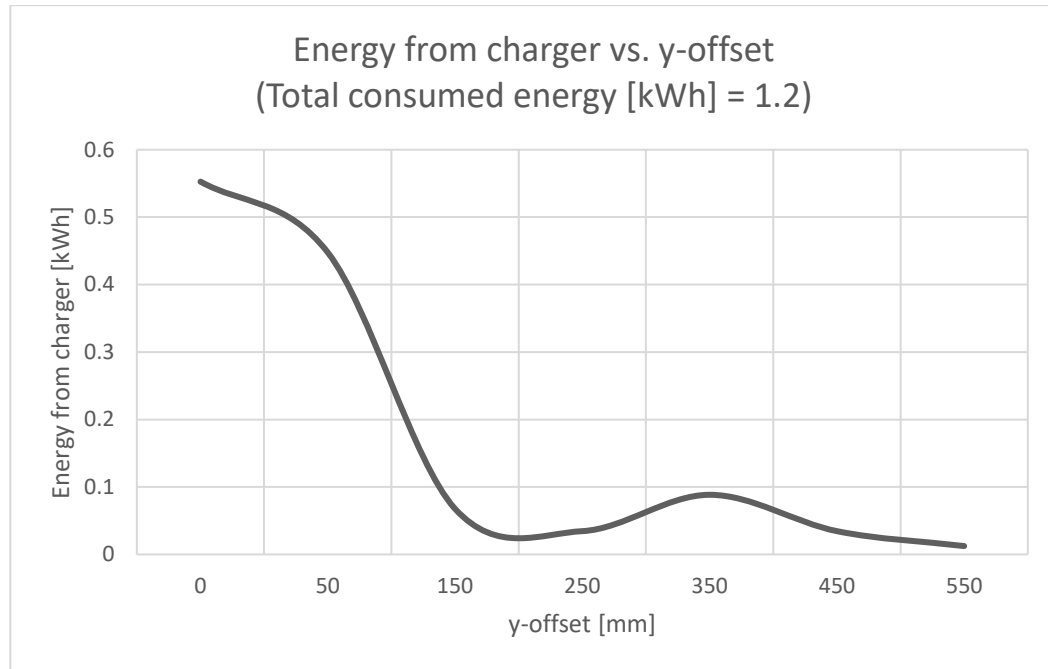


FIGURE 4.5 - ENERGY FROM CHARGER VS. Y-OFFSET

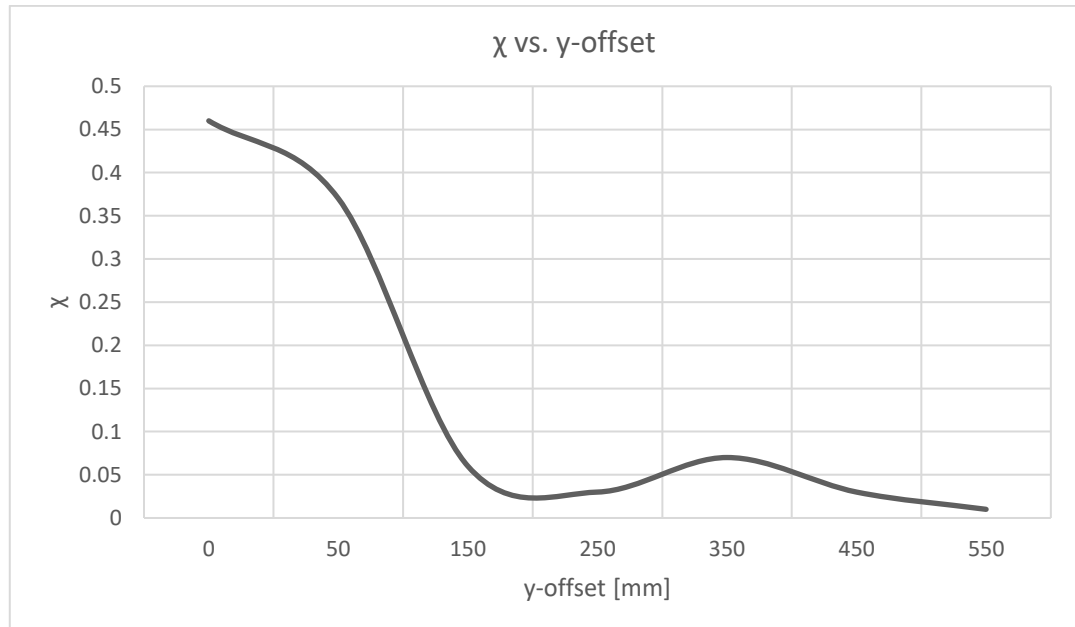


FIGURE 4.6 - χ VS. Y-OFFSET

As highlighted in Figure 4.5 in the range 0-150 mm the transferred energy considerably reduces (from 0.46 to 0.06 kWh) and for offsets higher than this value, as shown in Figure 4.6, the collected energy ratio is less than the 25% of the value in case of perfect alignment. With the hypothesis of containing the misalignment between 0 and 150 mm (quasi linear region of plot in Figure 3.12) along all the trip, a probabilistic relationship between speed and misalignment is here assumed (Figure 4.7).

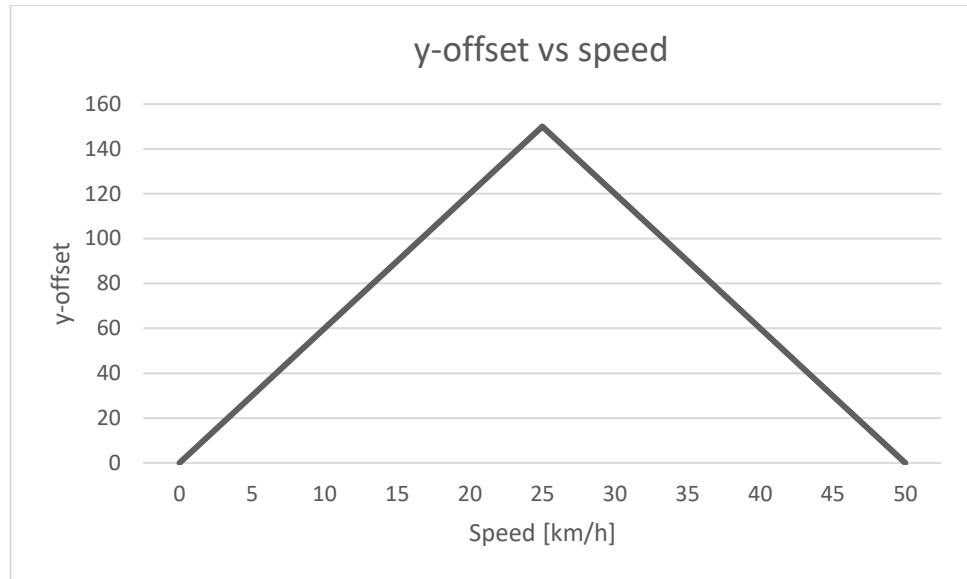


FIGURE 4.7 - Y-OFFSET VS. SPEED

The choice of a triangular relationship between speed and y-offset in the range 0-50 [km/h] is based on the following assumptions:

- Static/quasi-static region: the car is stopped or barely moving so a good alignment is considered more probable
- Low speed region: the car is turning or approaching a roundabout, probably with higher misalignment
- High speed: the number of changes of direction is limited hence a good alignment is achievable

With these assumptions the scenario changes compared to the constant misalignment situation:

Rua Carlos da Maia - Avenida de Madrid (Lisbon)				
Charging system: Table 4.11 (WPT3) – $\varepsilon=0.6075$				
Total consumed energy [kWh]: 1.2				
y-OFFSET [mm]	K_y	$M [\mu H]$	Energy from charger [kWh]	χ
0	1	18	0.5527	0.46
150	0.35	6.3	0.0677	0.06
Speed-based, range: 0-150	Avg: 0.89	Avg: 15.9	0.4664	0.39

TABLE 4.15 - X VALUE WITH Y-OFFSET BASED ON SPEED (AVG = AVERAGE)

5. Conclusions and future work

1.28 Conclusions and limitations of the model

As demonstrated by the results, dynamic wireless charging systems fit better in an urban environment. Average low speed and frequent stops mainly caused by intersections, could represent good chances for charging. On the contrary, on highways it would be necessary to cover longer paths to obtain a similar effect, with consequent higher costs.

The results also lead to a consideration on the possible targets of DWCSs. Nowadays, a normal private vehicle is parked for more than 90% of its life [51] and for the use that people make looks more interesting focusing on SWCSs. DWCSs can match better the needs of vehicles that move constantly at low speed and on pre-defined routes, for example public bus and taxi. Moreover, the sharing mobility that is quickly growing will likely make these solutions more attractive for public and private investments.

The main limit to the upscale of these systems to higher powers is given by the ability of the MV/LV grid (largely widespread in the cities) to absorb the frequent variations of load without compromising the use. In the railway sector, for instance, it is recommended to connect the feeding system to the stronger HV grid in order to reduce the effect of the disturbing load. The diffusion of smart grids could solve this problem. A communication system between the vehicles and the charging system could help managing the power requirements to the grid in order to make the load less variable.

In this context, this model is limited. Because of the linear proportionality between primary current and secondary voltage the values of current can be high in higher power cases. It neglects indeed the influence on the grid, the presence of harmonic components that could be injected and the overall reactive power of the system.

Another possible way to improve the charging process is modifying the track coverage ratio ϵ as demonstrated in chapter 4. A reduction of the distance between the coils generates a significant increase of the transmitted energy. By reducing even more D ($< 420mm$) it could be possible to assume that one receiving coil interacts with more transmitting coils amplifying the effect.

The parameter that mostly affects the energy transmission is the horizontal misalignment. As shown in chapter 4 a small increase in the lateral offsets leads to the fall of the transferred energy value. In a dynamic charging situation this matters more than in a static one. The

autonomous driving with its increasingly accurate lane-assistant systems could help solving this problem by keeping the car in the right trajectory to improve the charging process.

Another solution is offered by the geometry of the coils itself. By increasing the y-size of the DD coils it would be possible to reduce the effect of lateral misalignment.

A resume table of the effects and solutions of the different parameters is shown here.

PARAMETER	EFFECTS	SOLUTIONS
Average speed (U_{avg})	<ul style="list-style-type: none"> - $U_{avg} \uparrow, T \downarrow$ (on the charging track), $E \downarrow$. - It does not affect the “quality” of the transfer. - The more “static”, the better it is. 	<ul style="list-style-type: none"> - Always moving/low-speed vehicles (e.g., Bus, Taxi)
Available power (P_g)	<ul style="list-style-type: none"> - $P_g \uparrow, E \uparrow$. - Negative impact on the grid (disturbs). 	<ul style="list-style-type: none"> - Connection to HV grid - Smart grid balancing
Longitudinal displacement / Track coverage ratio (ϵ)	<ul style="list-style-type: none"> - $\epsilon \uparrow, E \uparrow$. - $\epsilon \uparrow$, increased interactions between transmitting and receiving coils. 	<ul style="list-style-type: none"> - WPT concentrated system with higher ϵ
Horizontal displacement / Horizontal alignment (K_y)	<ul style="list-style-type: none"> - $K_y \downarrow, M \downarrow, P_c \downarrow, E \downarrow$ - Low speed, higher probability of turns, traffic, roundabouts - It depends on the geometry of the coils (Y-size \uparrow, $K_y \uparrow$) 	<ul style="list-style-type: none"> - Working on the geometry of the coils (Y-size \uparrow) - Autonomous drive (lane assistant)

TABLE 5.1 - RESUME TABLE OF THE DIFFERENT PARAMETERS (\uparrow = “IF...INCREASES”, \downarrow = “IF...DECREASES”)

Future possible improvements of the work include:

- evaluating the effect of systems of this kind on the grid, such as disturbs and harmonic pollution
- testing the system with more than one vehicle charging track and its power managing

- designing a filtering system and a compensation network that could reduce the amount of Q in the system
- modifying the model considering other configurations, for instance a secondary-side power managing system with a DC-DC converter
- focus on the quest of a formulation for DD coils to calculate the parameters without the use of EMF simulations
- evaluating other geometries for coils to test their influence on the energy transmission
- evaluating the effect of the interaction of more transmitting coil with pick-up, studying the behaviour of the magnetic fields.

6. References

- [1] I. E. Agency, “Global Electric Vehicle Outlook 2022,” IEA, 2022.
- [2] International Electrotechnical Commission , “Technical Committee 69,” 2020.
- [3] A. Triviño-Cabrera, J. M. González-González and J. A. Aguado, Wireless Power Transfer for Electric Vehicles: Fundations ans Design Approach, Cham: Springer Nature Switzerland AG, 2020.
- [4] T. B. C. C. R. O’Sullivan, “Zebra battery technologies for all electric smart car,” *International Symposium on Power Electronics, Electrical Drives, Automation and Motion (IEEE)*, 2006.
- [5] C. B. C. J. B. Iclodean, “Comparison of different battery types for electric vehicles,” *IOP Conf. Ser.: Mater. Sci. Eng*, 2017.
- [6] The Boston Consulting Group, “Batteries for Electric Cars: Challenges, Opportunities, and the Outlook to 2020. Technical report.,” 2010.
- [7] M. R. S. Kumar, “Development scheme and key technology of an electric vehicle: an overview,” *Renew. Sustain. Energy*, 2017.
- [8] S. International, “SAE Electric Vehicle and Plug in Hybrid Electric Vehicle Conductive Charge Coupler J1772,” SAE International, 2017.
- [9] IEC, “IEC 61851 : Electric vehicle conductive charging system,” 2017. [Online].
- [10] K. L. K. P. Q. Z. C. Liu, “A brief review on key technologies in the battery management system of electric vehicles,” *Front. Mech. Eng*, 2019.
- [11] A. G.-G. J. A. J. Triviño, “Theoretical analysis of the efficiency of a V2G wireless charger for electric vehicles,” *Trans. Environ. Electr. Eng*, 2018.
- [12] Z. Popovic, “Cut the cord: low-power far-field wireless powering,” *IEEE Microw. Mag.*, 2013.
- [13] “IHS Markit | Leading Source of Critical Information,” [Online].
- [14] “Energy Research | Navigant Research,” [Online].
- [15] Z. Z. Y. K. T. L. F. Z. K. S. B. M. C. Yan, “Frequency optimization of a loosely coupled underwater wireless power transfer system considering eddy current loss,” *IEEE Trans. Ind. Electron*, 2019.

- [16] S. C. X. A. I. G. W. Kisseleff, "Efficient charging of access limited wireless underground sensor networks," *IEEE Trans. Commun.*, 2016.
- [17] H. H. H. K. S. H. K. Z. R. C. J. Kim, "Review of near-field wireless power and communication for biomedical applications," *IEEEAccess*, 2017.
- [18] K. N. S. J. S. W. L. Lu, "Design of auto frequency tuning capacitive power transfer system based on class-E2 dc/dc converter," *IET Power Electron.*, 2017.
- [19] W. M. C. Zhang, "Compensation topologies of high-power wireless power transfer systems," *IEEE Trans. Veh. Technol.*, 2016.
- [20] G. S. J. C. A. C. D. F. N. P. G. S. Di Capua, "losses-based analysis for electric vehicle wireless chargers.," *International Conference on Synthesis, Modeling, Analysis and SimulationMethods and Applications to Circuit Design (SMACD)*, 2015.
- [21] V. Murugan, R. Narayananamoorthi, V. Pradeep and B. Mohit, "A Review of Compensation Topologies and Control Techniques of Bidirectional Wireless Power Transfer Systems for Electric Vehicle Applications," *MDPI*, 2022.
- [22] Bombardier, "BOMBARDIER PRIMOVE to Provide Wireless Charging and Battery Technology to Berlin - Bombardier," 2015. [Online].
- [23] WIRED, "Electric Buses Test Wireless Charging in Germany," 2013. [Online].
- [24] C. B. G. C. S. R. C. Mi, "Modern advances in wireless power transfer systems for roadway powered electric vehicles," *IEEE Trans. Ind. Electron.*, 2016.
- [25] Eltis, "Wireless charging for quiet and clean public transport in Torino (Italy)," [Online].
- [26] IEEE, "An Electric Roadway System Leveraging Dynamic Capacitive Wireless Charging: Furthering the Continuous Charging of Electric Vehicles," *IEEE Electrification Magazine*, 2020.
- [27] G. Fumarola, "Panoramica sulla tecnologia di ricarica dinamica wireless: stato dell'arte e implementazioni future," Padova, 2020.
- [28] SAE, "Surface Vehicle Standard J2954 - Wireless Power Transfer for Light-Duty Plug-in/Electric Vehicles and Alignment Methodology," SAE, 2020.
- [29] IEC, IEC 61980-1:2020, Electric vehicle wireless power transfer (WPT) systems - Part 1: General requirements, 2020.
- [30] Z. W, Z. T, G. Q, S. L, Z. N, J. X and Y. J, "High-efficiency wireless power transfer system for 3D, unstationary free-positioning and multi-object charging," *IET Electr. PowerAppl.*, 2018.

- [31] Y. L. X. P. F. Z. H. G. Z. Y. T. Li, "Wireless energy transfer system based on high Q flexible planar-Litz MEMS coils," in *The 8th Annual IEEE International Conference on Nano/Micro Engineered and Molecular Systems*, 2013.
- [32] K. F. B. Fotopoulou, "Wireless power transfer in loosely coupled links: coil misalignment," *IEEE Trans*, 2011.
- [33] Z. W. X. Luo, "Analysis of square and circular planar spiral coils in wireless power transfer system for electric vehicles," *IEEE Trans*, 2018.
- [34] M. B. J. C. G. H. C. Budhia, "Development of a single-sided flux magnetic coupler for electric vehicle IPT charging systems," *IEEE Trans*, 2013.
- [35] G. C. G. B. J. Nagendra, "Determining the physical size of inductive couplers for IPT EV systems," *IEEE J. Emerg. Sel. Top. Power Electron*, 2014.
- [36] J. C. G. Boys, "The inductive power transfer story at the University of Auckland," *IEEE Circuits Syst. Mag*, 2015.
- [37] A. B. E. J. C. Rosskopf, "Influence of inner skin- and proximity effects on conduction in litz wires," *IEEE Trans. Power Electron*, 2014.
- [38] R. K. M. Wojda, "Winding resistance and power loss of inductors with litz and solid-round wires," *IEEE Trans. Ind. Appl*, 2018.
- [39] MRFR, "Market Research Future: Wireless Power Transmission Market Research Report - Forecast 2022," 2019.
- [40] N. Research, "The Disruptive Potential of Wireless EV Charging," 2018.
- [41] J. M. F. T. V. d. Carvalho, "Avaliacao dos sistemas de carregamento wireless do ponto de vista da transferencia de energia em mobilidade elétrica," IST, Lisboa, 2022.
- [42] N. Mohan, T. M. Undeland and W. P. Robbins, *Power Electronics*, 3rd edition, John Wiley & Sons, Inc, 2003.
- [43] P. Steven and S. Timothy, "ACSL/Graphic Modeller Component Models for Electric Power Education," IEEE, 1998. [Online].
- [44] M. Bertoluzzo, "STUDIO E PROGETTO PRELIMINARE PER UN SISTEMA DI RICARICA DINAMICA WIRELESS," ENEA, 2016.
- [45] G. Buja, M. Bertoluzzo, H. Kumar and Dashora, "Lumped Track Layout Design for Dynamic Wireless Charging of Electric Vehicles," *IEEE TRANSACTIONS ON INDUSTRIAL ELECTRONICS*, October 2016.
- [46] "Scenes, rectifying the future," [Online].

- [47] Z. -. G. E. a. E. M. Association, "Voltage Casses for Electric Mobility," 2013.
- [48] G. Buja and M. Bertoluzzo, "Studio e progetto preliminare per un sistema di ricarica dinamica wireless," *ENEA - Ricerca di sistema elettrico*, 2016.
- [49] KIA, "www.KIA.com," [Online].
- [50] "Google API," Google. [Online].
- [51] M. Grassi, "Motor 1," 28 June 2022. [Online]. Available: <https://it.motor1.com/news/594800/auto-condivisa-elettrica-futuro/>.
- [52]
- [53] H. c. projects, "Simple Buck-Boost Converter Circuits Explained," [Online].
- [54] Google, "Maps," Google. [Online].
- [55] C. Fuhai, W. Pan, S. Chenglong, W. Yuming, D. Zhenlan, X. Chenjin, W. Shuo and W. Wei, "Research on Optimization of Horizontal Omnidirectional Misalignment Tolerance of WPT Based on Double D Coupler," *MDPI electronics*, 2022.

Acknowledgments

Quero agradecer a Doutora Patrícia Baptista e o Doutor Gonçalo Duarte pela ajuda que forneceram para a conclusão deste trabalho. Tornaram a minha experiência de Erasmus ainda melhor.

Queria agradecer la Profesora Alicia Triviño-Cabrera por los datos fundamentales que me ha amablemente servido.

Ringrazio la mia famiglia per la pazienza e per avermi dato la possibilità di compiere questo percorso. Avreste meritato un figlio/fratello/nipote/cugino migliore.

Ringrazio i miei amici di sempre per avermi sempre preso in giro. Finalmente potrò cambiarvi le lampadine con titolo.

I am grateful to my Erasmus friends for helping me not to write this thesis. Thanks for the unforgettable memories.